Electronic Supplementary Material (ESI) for ChemComm.

High MOF loading in mixed-matrix membranes utilizing styrene/butadiene copolymers

Jessica. C. Moreton, Michael S. Denny, Jr., and Seth M. Cohen*

Department of Chemistry and Biochemistry, University of California, San Diego, La Jolla, California 92093, United States

SUPPORTING INFORMATION

Experimental

Materials

All solvents and starting materials were purchased from chemical suppliers and used without further purification (Sigma Aldrich, Alfa Aesar, EMD, and TCI).

Synthetic Procedures

Synthesis of UiO-66: Zirconium(IV) chloride (61 mg, 0.26 mmol) and terephthalic acid (43 mg, 0.26 mmol) were dissolved in 15 mL DMF with 0.45 mL glacial acetic acid in a 20 mL vial with Teflon-lined cap. The vial was then placed in a 120 °C oven for 24 h. After cooling to ambient temperature, the particles were collected by centrifugation (fixed-angle rotor, 6000 rpm, 5 min), followed by washing with 3×10 mL DMF and 3×10 mL MeOH. The particles were then soaked in MeOH for 3 d, with solvent changed daily, before being dried under vacuum at room temperature.

Synthesis of UiO-66-NH_2: Zirconium(IV) chloride (61 mg, 0.26 mmol) and 2-aminoterephthalic acid (43 mg, 0.26 mmol) were dissolved in 15 mL DMF with 0.45 mL glacial acetic acid in a 20 mL vial with Teflon-lined cap. The vial was then placed in a 120 °C oven for 24 h. After cooling to ambient temperature, the particles were collected by centrifugation (fixed-angle rotor, 6000 rpm, 5 min), followed by washing with 3×10 mL DMF and 3×10 mL MeOH. The particles were then dispersed in MeOH (10 mg/mL concentration) and heated to reflux for 24 h, before being dried under vacuum at room temperature.

Film Fabrication: UiO-66 was synthesized according to the procedure reported above, then dispersed in a 1:1 THF/Ethyl acetate solution at a concentration of 200 mg/mL via sonication. Polymers were dissolved in THF, (**PS =** 220 mg/mL, **SBS** = 100 mg/mL, **SBR** = 50 mg/mL) then the MOF and polymer solutions were mixed (proportions dictated by final wt% of MOF desired), sonicated, and doctor-bladed onto aluminum foil. Using the draw-down method, the MOF/polymer solution was transferred to an aluminum foil substrate and then cast with a MTI Corporation MSK-AFA-II automatic thick film coater using an adjustable doctor blade set to a height of 500 μm at a speed of 25 mm/second. The cast films were then oven-cured at 55 °C until dry, for 3 h (drop-cast) or 30 min (doctor-bladed) and the aluminum backing was peeled away with tweezers. Although the technique is inherently scalable, most MMMs fabricated comprised a total of 200-500 mg of combined MOF and polymer components and were roughly 3×5 in. (200 mg material) to 5×8 in. (500 mg material) in size.

Dye Filtration Experiment: A 13mm diameter circle of 80 wt% UiO-66/**SBS** MMM was placed in 13 mm Swinnex® syringe filters, and 2.5 mL of 10 μM dye was filtered through the membrane at a speed of 0.1 mm/min in a dead-stop filtration setup. The filtrate was collected and analyzed by UV-Vis spectrophotometry at the peak visible absorption of each dye, and residual dye content was calculated relative to initial dye concentrations. For Coomassie Brilliant Blue R-250, λ_{max} = 555 nm. For Methyl Orange, λ_{max} at pH 7 = 465 nm. For recyclability measurements, the MMMs were removed from the syringe filter housings and soaked in methanol for roughly 1 h. The MMMs were then dried in air for roughly 1 h, replaced in the syringe filter housings, and re-challenged by the same procedure.

MOF and film digestion for NMR: 10 mg of UiO-66, UiO-66-NH_2, or the equivalent weight of MMM were dispersed in 590 μL of DMSO-d_6, then 10 μL of HF was added. MOF mixtures

were sonicated for 30 min to fully dissolve the MOF for analysis by NMR. MMMs were allowed to digest without sonication over a period of 12 h, over the course of which the MMMs change from opaque to transparent; the DMSO-d_6 solution was then analyzed by NMR.

PSM with Acetic Anhydride: Three pre-cut strips of 80 wt% UiO-66-NH_2/**SBS** MMM (roughly 2×10 cm^2 in size) were suspended in 100 mL neat acetic anhydride and heated at 60 °C for 24 h. The MMMs were then soaked and rinsed in MeOH for 3 d, and dried at ambient temperature overnight. The 2×10 cm^2 strips fragment during reaction, yielding MMMs roughly 2×3cm^2 in size. Small portions were digested via the procedure given above and analyzed by ^{1}H NMR. The experiment was simultaneously conducted on ~80 mg of the pure UiO-66-NH_2 MOF and ~20 mg pure **SBS** as controls, as well as 80 wt% UiO-66/**SBS** MMMs, to assess the effect of the reaction conditions on a non-reactive MMM. Integration analysis of 2-aminoterephthalic acid peak areas compared to acetylated 2-aminoterephthalic acid peak areas in the phenyl region show that both UiO-66-NH_2 and the 80 wt% MMM tested both achieve >95% conversion to the acetylated product. Control experiments, with pure **SBS** membranes and the 80 wt% UiO-66/**SBS** MMMs generated no reaction products as gauged by NMR. The pure **SBS** membrane (~100 μm in thickness) showed no physical degradation in the reaction conditions. However, the 80 wt% UiO-66/**SBS** MMMs fragment in the reaction conditions similar to the 80 wt% UiO-66-NH_2-based MMM, despite the lack of a PSM reaction in this MMM. Therefore, the fragmentation of the MMMs is attributed to degradation of the polymer component of the MMMs under the PSM reaction conditions that appears to be exacerbated by the presence of the MOFs.

PSE with 2-Aminoterephthalic Acid: 50 equivalents (2 mmol) of 2-aminoterephthalic acid was dissolved and deprotonated in 100 mL of 4 wt% aqueous KOH solution, then neutralized to

pH 7 with 6M HCl. To this solution was added 30 equivalents of UiO-66 in MMM form (80 wt% UiO-66/**SBS**, 300 mg of film). The solution was heated to 60 °C for 24 h, then the film was rinsed in MeOH for 3 d. Small portions of the MOF were digested by the procedure given above and analyzed by ^{1}H NMR. The experiment was simultaneously conducted on ~80mg of the pure MOF and ~20mg of the pure **SBS** as controls. Integration analysis of terephthalic acid peak areas compared to 2-aminoterephthalic acid peak areas in the phenyl region show that UiO-66 alone achieves 47% conversion in the control experiment, while the 80 wt% MMM tested achieves 17% exchange with the 2-aminoterephthalate linker. The pure **SBS** control generated no products under the same digestion conditions as gauged by NMR, and showed no obvious physical degradation.

Materials Characterization

Powder X-ray Diffraction (PXRD): PXRD data was collected at room temperature on a Bruker D8 Advance diffractometer running at 40 kV, 4 mA for Cu Kα (λ = 1.5418 Å), with a scan speed of 0.2 sec/step, a step size of 0.02° in 2θ, and a 2θ range of 5-50° at room temperature.

N_2 Sorption Analysis: ~50-100 mg of sample were placed in a tared sample tube and degassed at 105 °C overnight on a Micromeritics ASAP 2020 Adsorption Analyzer until the outgas rate was <5 mmHg. Post-degas, the sample tube was weighed, and then N_2 sorption data with BET analysis was collected at 77 K on a Micromeritics ASAP 2020 Adsorption Analyzer using a volumetric technique. BET surface areas were then determined from analysis of the Rouquerol plots of the isotherm data, using ten data points each. The guidelines set forth by Rouquerol[1] use

four criteria to obtain the most accurate BET surface area values for microporous materials, such as MOFs. Further work by Snurr,[2] specific to UiO-66, recommends the implementation of criteria I and II to obtain the most accurate BET surface area measurement for this specific material (because criteria III and IV are not met in UiO-66).[2] Criteria I, that BET constant C must be positive, and criteria II, that the value $V(1\text{-}p/p_0)$ must increase with increasing p/p_0 for all points chosen, are both true for the UiO-66 and MMMs in this study (see Table S2 and Figure S19). Pore size distributions were calculated using the DFT method.

Scanning Electron Microscopy (SEM): MMMs were placed on conductive carbon tape on a sample holder and coated using an Ir-sputter coating for 8 s. A Phillips XL ESEM microscope was used for acquiring images using a 15 kV energy source under vacuum at a working distance of 10 mm.

Nuclear Magnetic Resonance Spectroscopy (NMR): ^{1}H NMR were recorded on a Varian FT-NMR spectrometer (400 MHz). Chemical shifts are quoted in parts per million (ppm) referenced to the appropriate solvent peak or 0 ppm for TMS.

Mechanical Testing: Tensile strength measurements were conducted according to ASTM Standard D882- 02 using an Instron® Universal Testing Machine (3342 Single Column Model) with a 500N load cell in extension mode. Tensile measurements were acquired at an extension rate of 0.005 mm/s with a sampling rate of 500 ms to generate stress-strain curves, then ultimate tensile strength and elastic modulus were calculated using MS Excel. Sample thicknesses were measured using a Mitutoyo Digital Micrometer (0-25 mm range, 0.001 mm resolution, IP 54 standard) and averaged from 5 independent measurements from each sample. Tensile data were collected for at least 3 independent samples.

Tables and Figures

Table S1. BET surface area measurements on all membranes show that below 70 wt% MOF loading, none of the surface area of the MOF is retained. At and above 70 wt%, surface area is partially recovered.

Polymer	% MOF	BET Surface Area, m^2/g
N/A	100	1214±44
PS	0	< 5
	30	< 5
	50	< 5
	70	779±114
SBS	0	< 5
	30	< 5
	40	< 5
	50	< 5
	60	< 5
	70	578±182
	80	774±32
	90	781±48
SBR	0	< 5
	30	< 5
	50	< 5
	70	737±248

Table S2. BET constants for several MMMs corresponding to the representative Rouquerol plots in Figure S19. Positive values of C indicate compliance with criteria I.

Polymer	% MOF	BET constant C	BET constant Q_m (cm^3/g STP)
N/A	100	5127	269
SBS	70	8018	174
	80	5236	179
	90	5411	189
PS	70	6608	203
SBR	70	8828	225

Table S3. Ultimate tensile strength (UTS) and elastic modulus (in megapascals, Mpa) values for several MMMs. Note: values for PSE reacted MMMs are the average of two measurements.

Sample	Ultimate Tensile Strength (MPa)	Elastic Modulus (MPa)
70 wt% MOF/**SBR**	0.17 ± 0.21	44 ± 42
0 wt% MOF/**SBS**	0.73 ± 0.1	53 ± 7
30 wt% MOF/**SBS**	1.57 ± 0.25	128 ± 28
50 wt% MOF/**SBS**	1.76 ± 0.12	387 ± 78
70 wt% MOF/**SBS**	0.93 ± 0.03	248 ± 47
80 wt% MOF/**SBS**	0.97 ± 0.22	209 ± 47
Post-PSE 80 wt% MOF/**SBS**	0.37 ± 0.04	131 ± 38

Table S4. BET surface area measurements on PSM and PSE treated MMMs as compared to pure MOF controls subjected to the same reaction conditions. Note: all BET surface areas reported below are calculated using data that complies with Rouquerol criteria I and II (see above).

Reaction	Species	BET Surface Area, m^2/g	Ratio of MMM:MOF S.A.
Postsynthetic Modification (PSM)	80 wt% UiO-66-NH_2/**SBS**	425±5	~0.5
	UiO-66-NH_2	841±5	
Postsynthetic Exchange (PSE)	80 wt% UiO-66/**SBS**	607±5	~0.55
	UiO-66	1104±3	
No Reaction	80 wt% UiO-66/**SBS**	774±32	~0.6
	Pure UiO-66	1214±44	

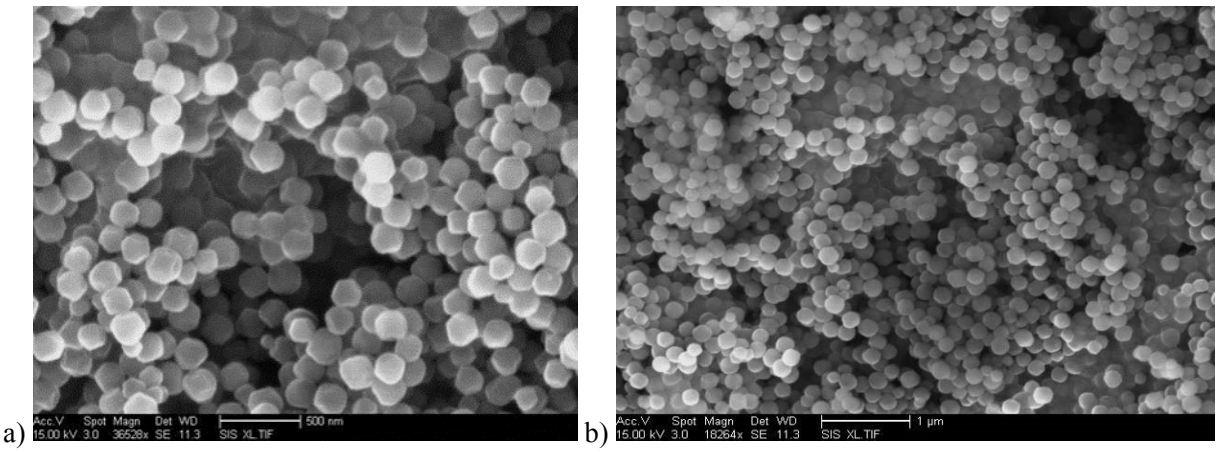

Figure S1. SEM images of as-synthesized UiO-66 at two different magnifications (scale bars of 500 nm and 1 μm on the left and right, respectively). These images highlight the uniform ~200 nm diameter size and truncated octahedral morphology of the particles.

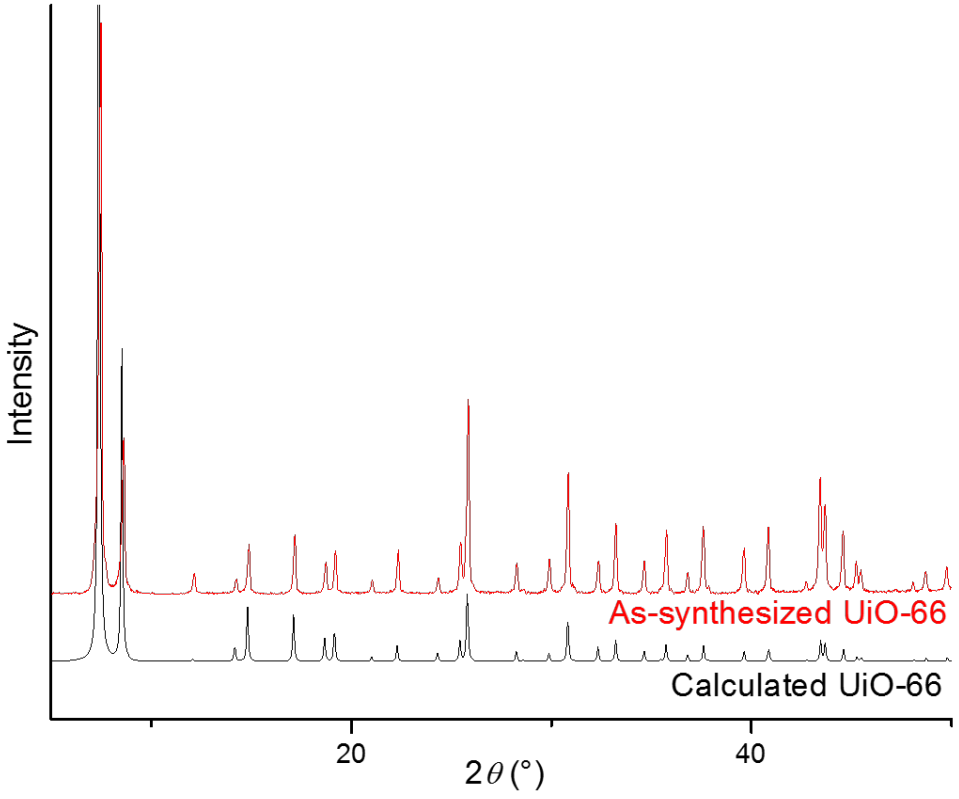

Figure S2. PXRD of as-synthesized UiO-66 used in this study with the calculated powder pattern for comparison.

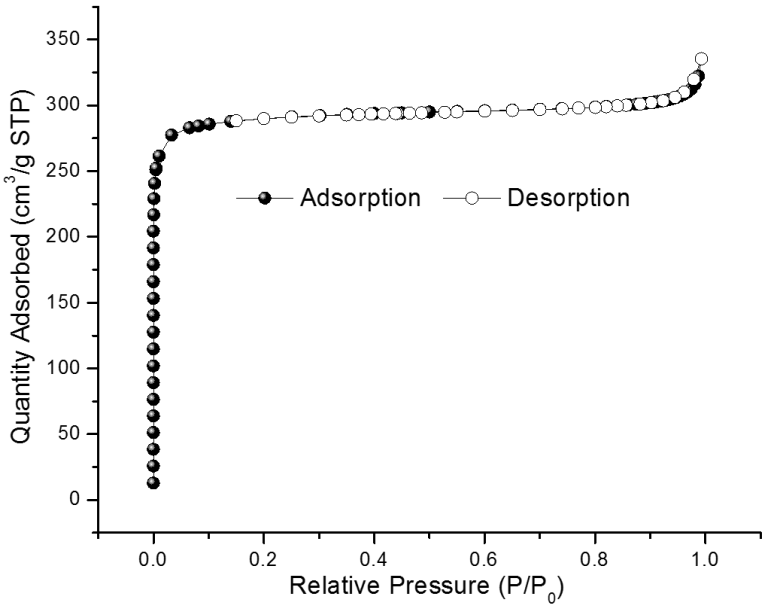

Figure S3. Nitrogen sorption isotherm data of as-synthesized UiO-66 used in this study.

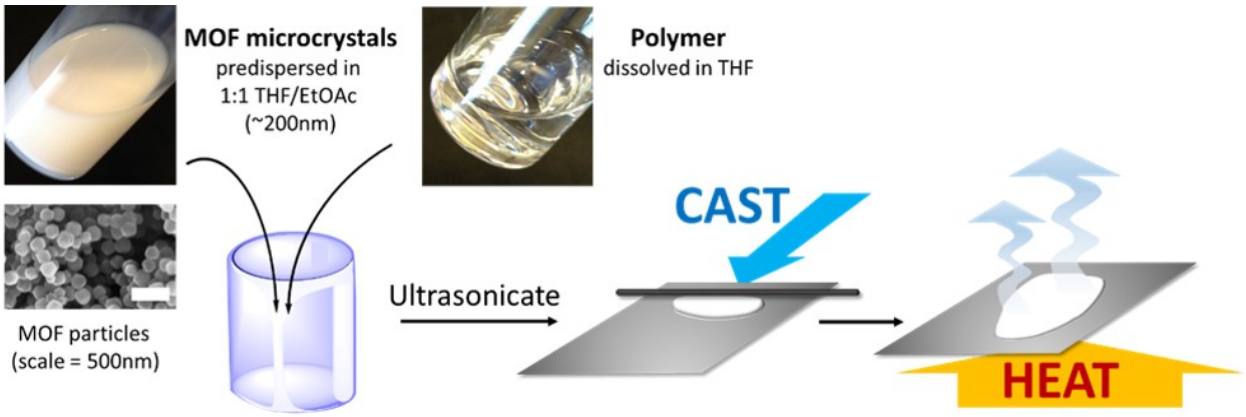

Figure S4. Diagram of MMM casting procedure. First, the MOF and polymer are dispersed separately in solvent, then the solutions are combined and ultrasonicated to create a viscous liquid. This solution is then cast on an aluminum foil substrate and heated in a 55 °C oven to drive off solvent. The resulting MMM can then be mechanically delaminated.

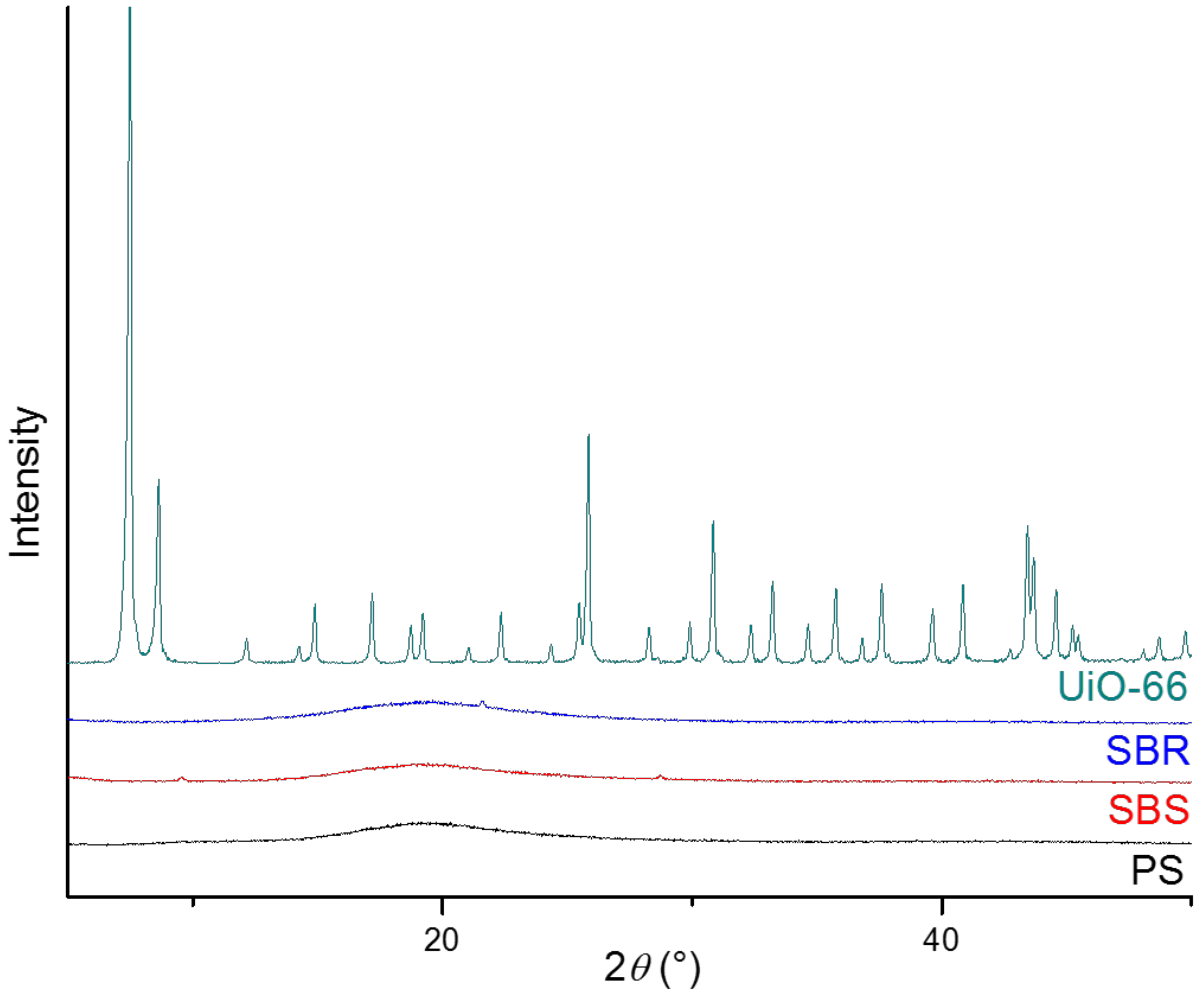

Figure S5. PXRD patterns of polymers as compared to UiO-66. The polymers alone display amorphous character, with only a small feature at $2\theta = \sim 19°$.

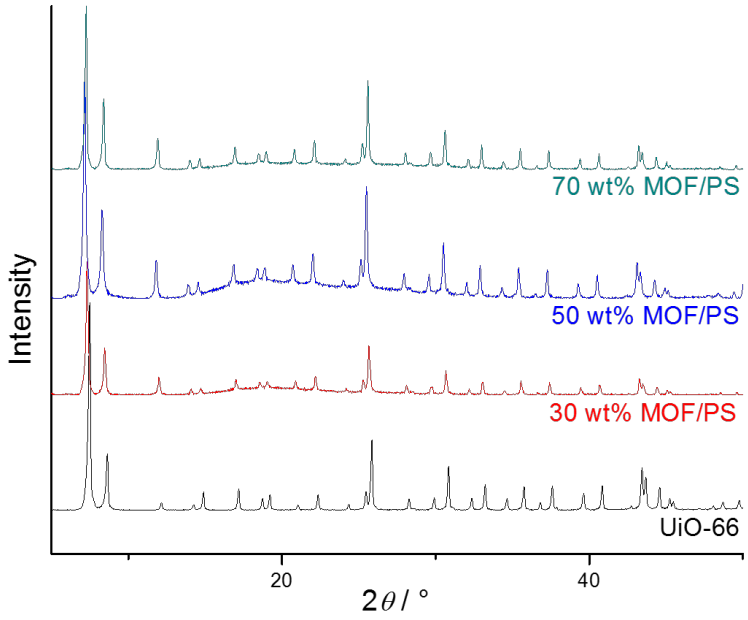

Figure S6. PXRD patterns of UiO-66/**PS** MMMs at the indicated wt% loadings. All powder patterns show that UiO-66 remains highly crystalline within the MMMs.

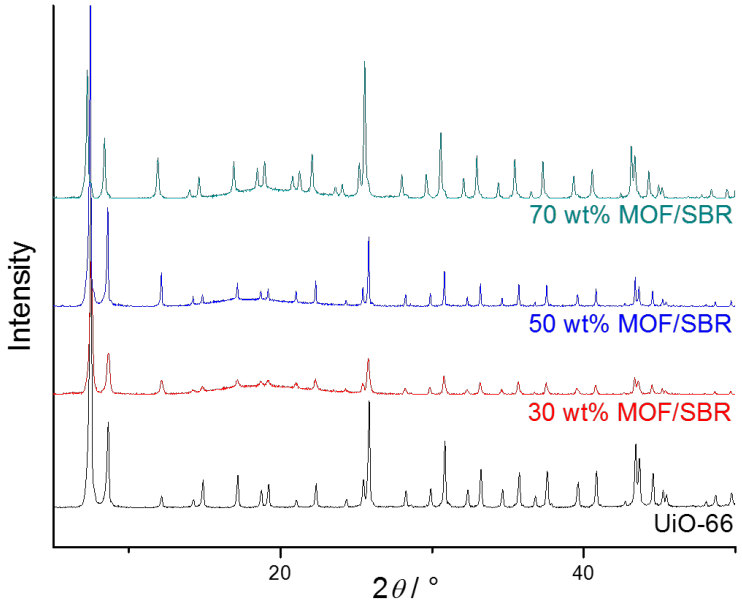

Figure S7. PXRD patterns of UiO-66/**SBR** MMMs at the indicated wt% loadings. All powder patterns show that UiO-66 remains highly crystalline within the MMMs.

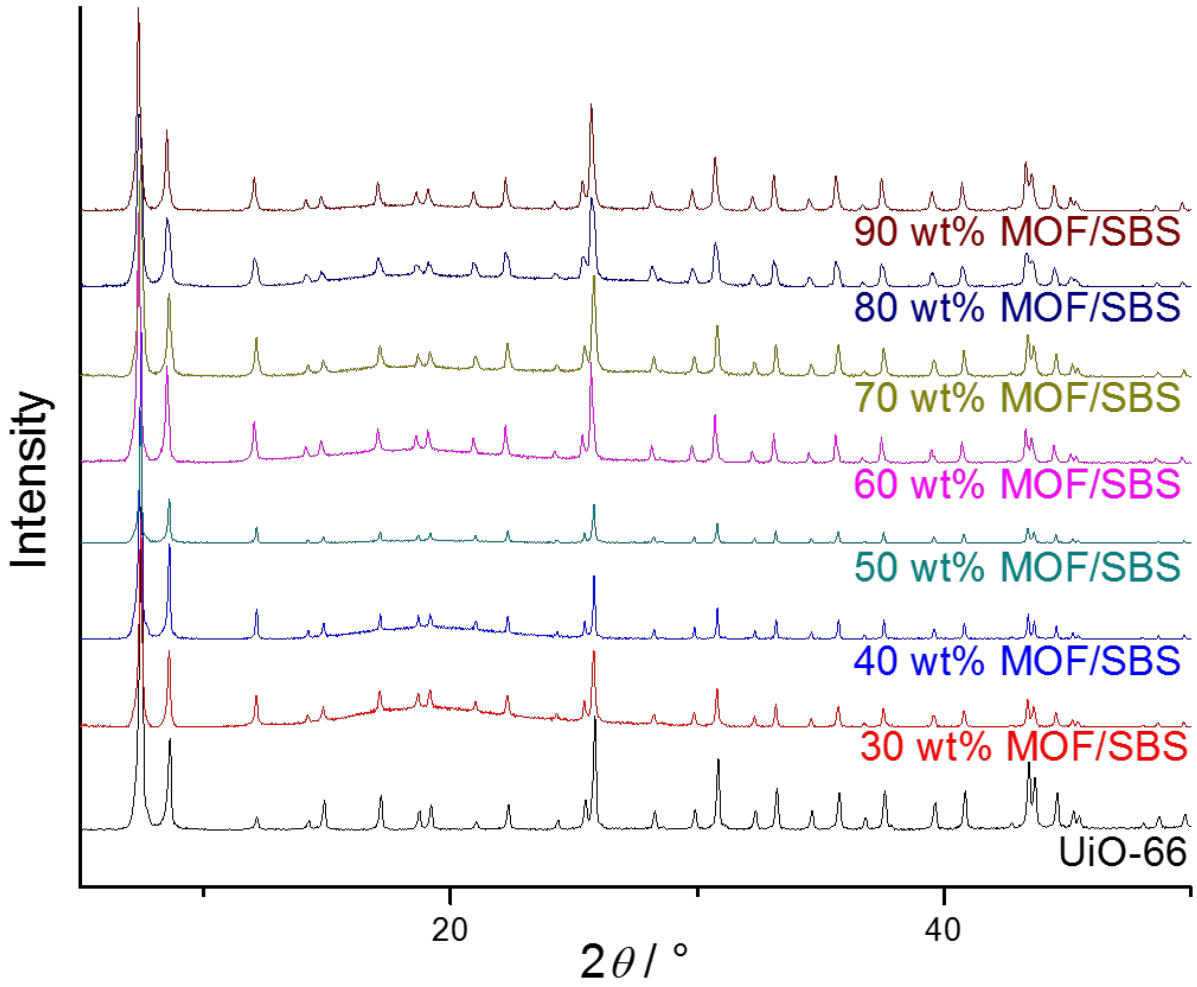

Figure S8. PXRD patterns of UiO-66/**SBS** MMMs at the indicated wt% loadings. All powder patterns show that UiO-66 remains highly crystalline within the MMMs.

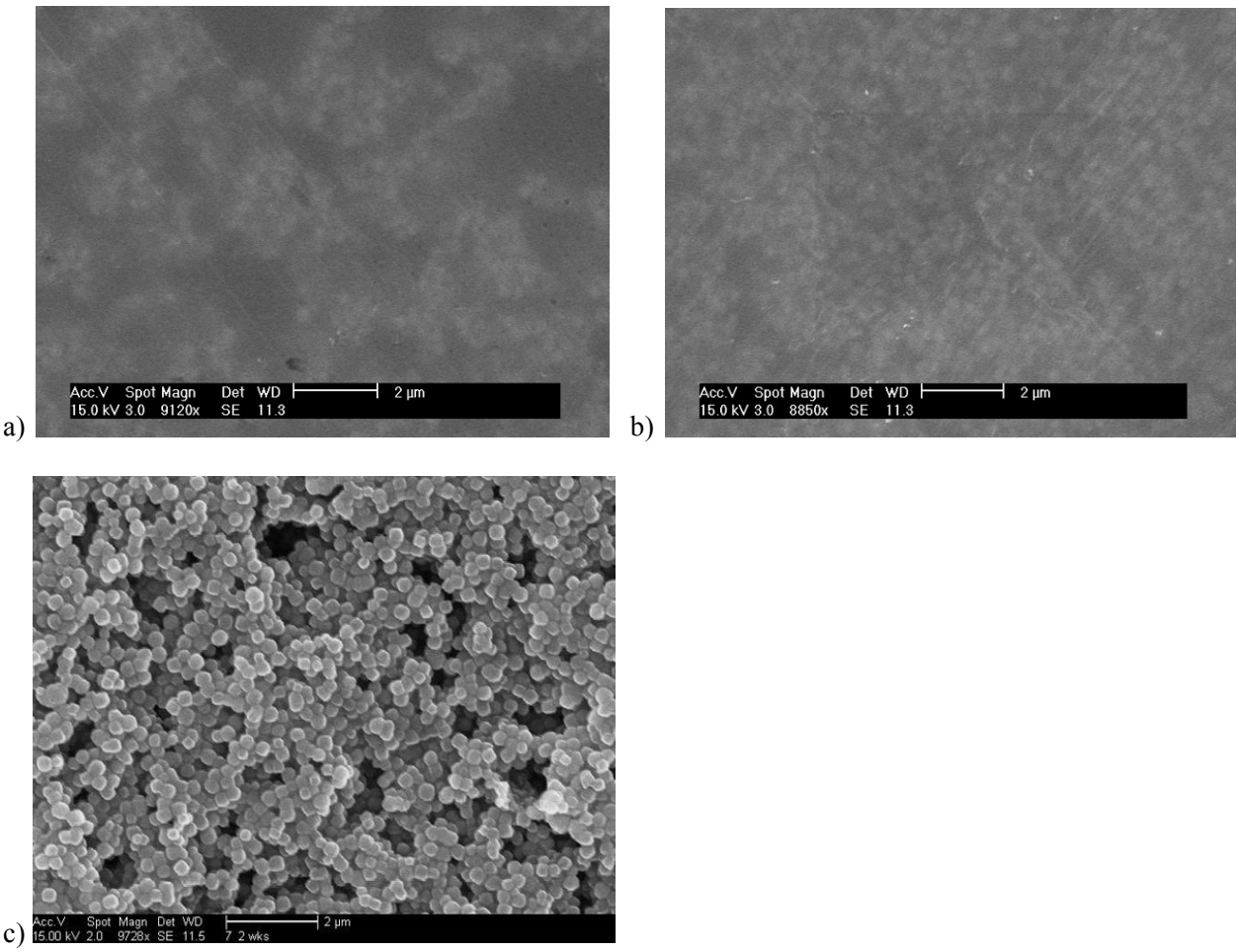

Figure S9. SEM top-down images of UiO-66/**PS** MMMs show increasing UiO-66 content uniformly encased in polymer at a) 30 and b) 50 wt% loadings. At c) 70 wt% loadings, the MOF appears more isolated and film surfaces roughen accordingly. All scale bars are 2 µm.

a) 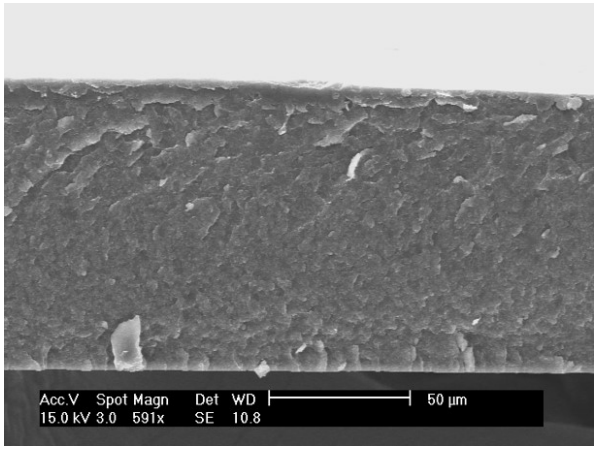

b) 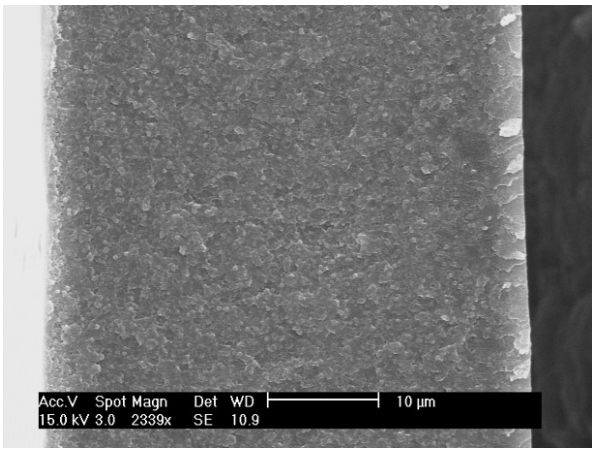

c) 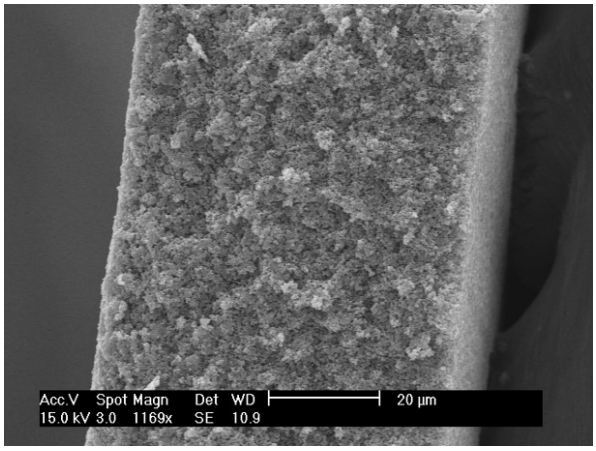

Figure S10. SEM cross-section images of UiO-66/**PS** MMMs show increasing UiO-66 content uniformly dispersed in polymer at: a) 30 (scale bar = 50 µm), b) 50 (scale bar = 10 µm), and c) 70 wt% (scale bar = 20 µm) loadings.

a) 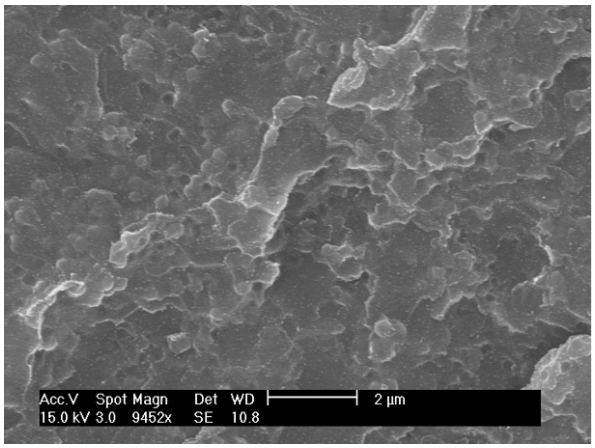

b) 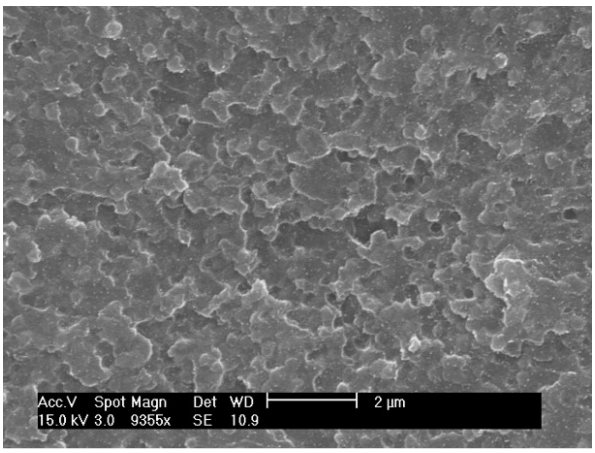

c) 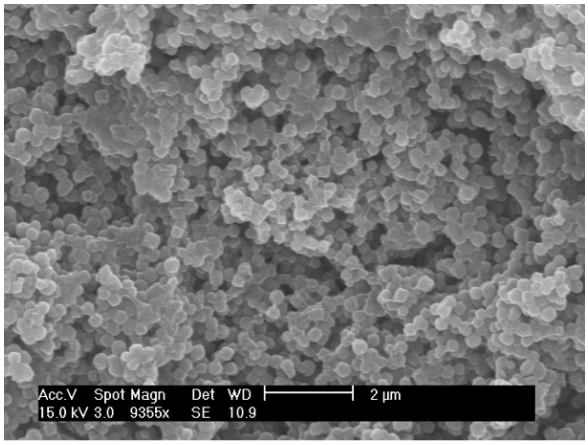

Figure S11. SEM cross-sectional zoomed-in images of UiO-66/**PS** MMMs show increasing UiO-66 content uniformly encased in polymer at a) 30 and b) 50 wt% loadings. At c) 70 wt% loadings, the MOF appears more isolated, showing a much more porous overall morphology throughout the cross-section. All scale bars are 2 µm.

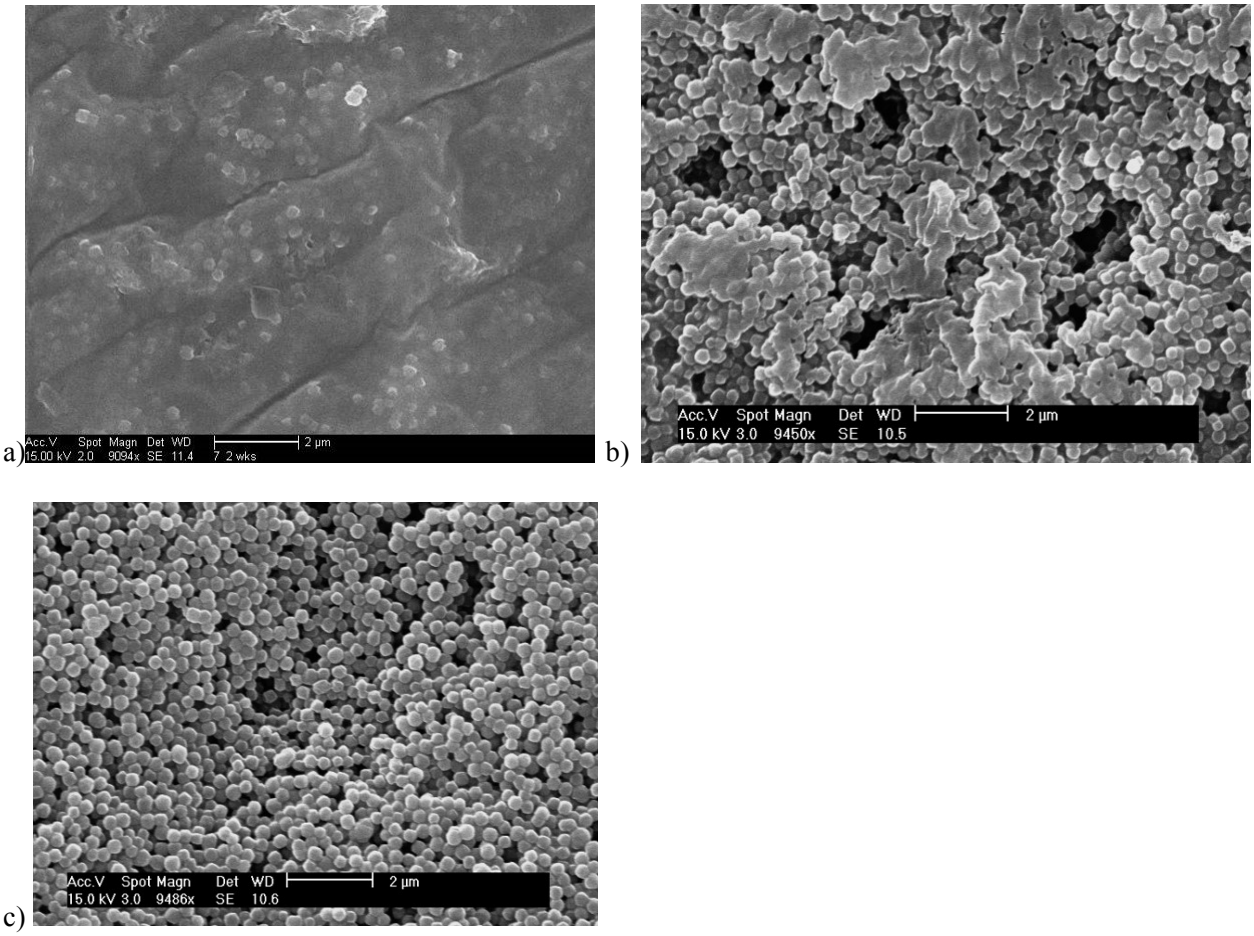

Figure S12. SEM top-down images of UiO-66/**SBR** MMMs show UiO-66 particles dispersed in polymer. At a) 30 wt% loading, MOF particles are encased in polymer. As MOF loading increases in b) 50 wt% and c) 70 wt%, the MOF appears far more isolated and film surfaces roughen accordingly. All scale bars are 2 µm.

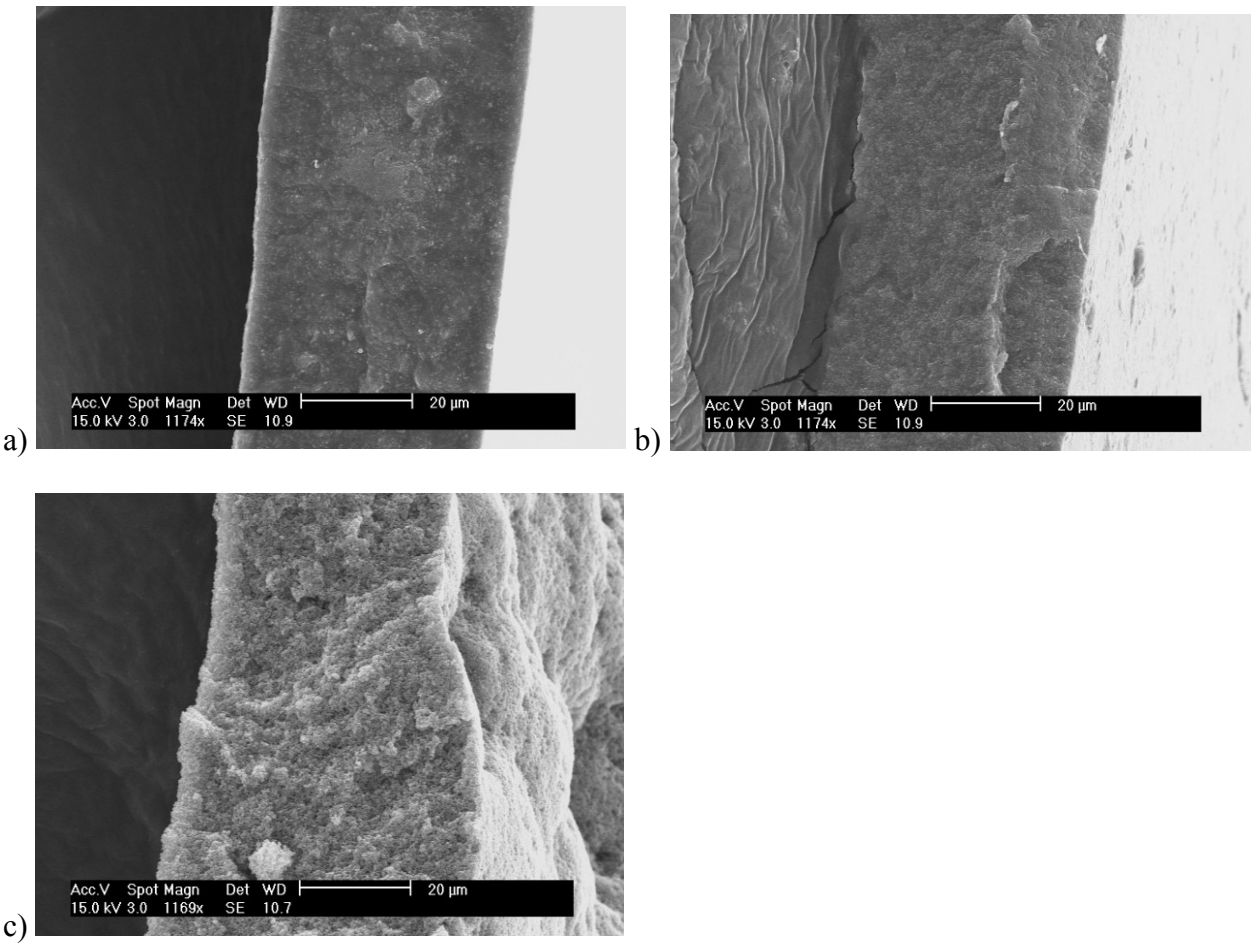

Figure S13. SEM cross-sectional images of UiO-66/**SBR** MMMs show increasing UiO-66 content uniformly dispersed in polymer at a) 30, b) 50 and c) 70 wt% loadings. All scale bars are 20 µm.

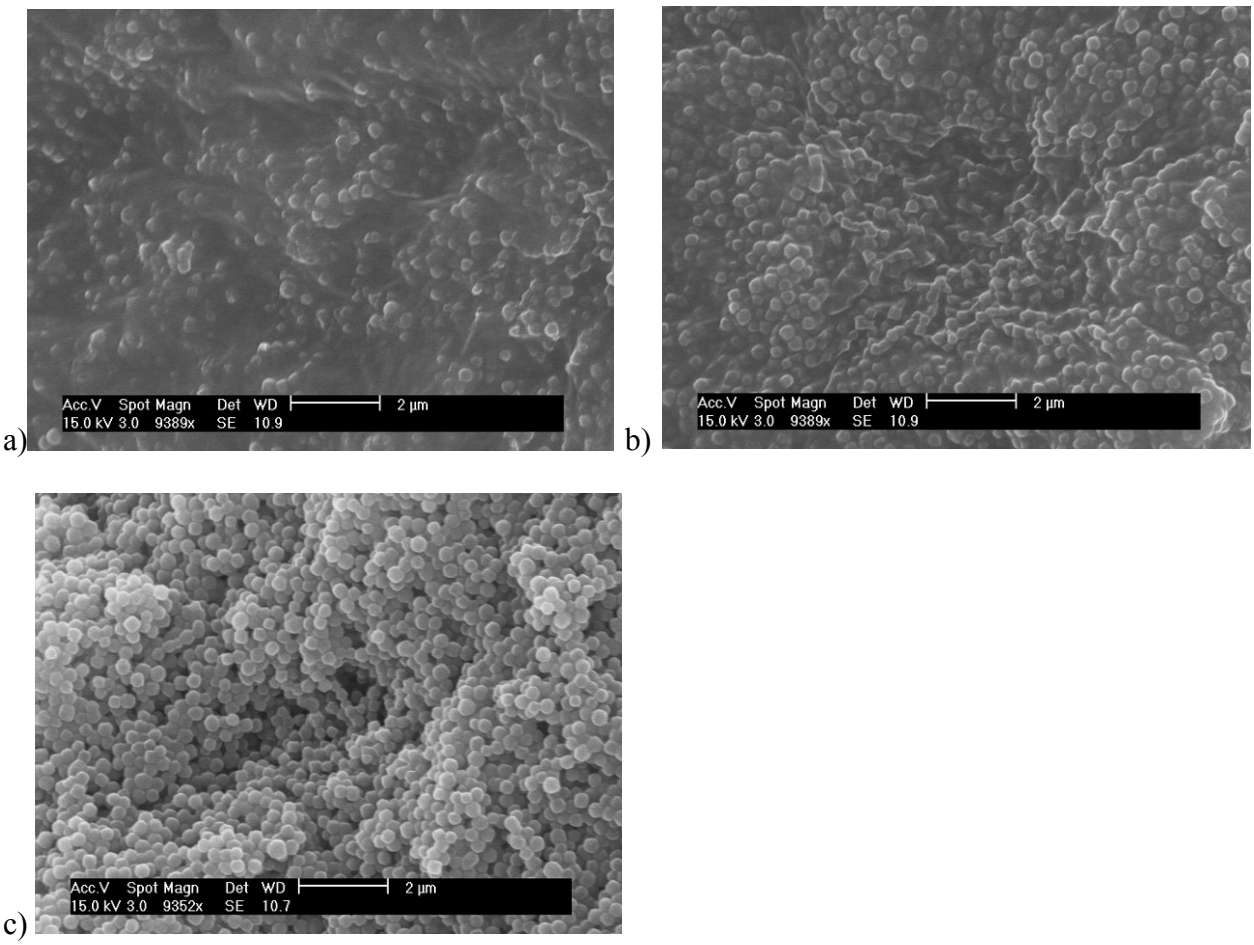

Figure S14. SEM cross-sectional zoomed-in images of UiO-66/**SBR** MMMs show increasing UiO-66 content uniformly encased in polymer at a) 30 and b) 50 wt% loadings. At c) 70 wt% loadings, the MOF appears more isolated, showing a much more porous overall morphology throughout the cross-section. All scale bars are 2 µm.

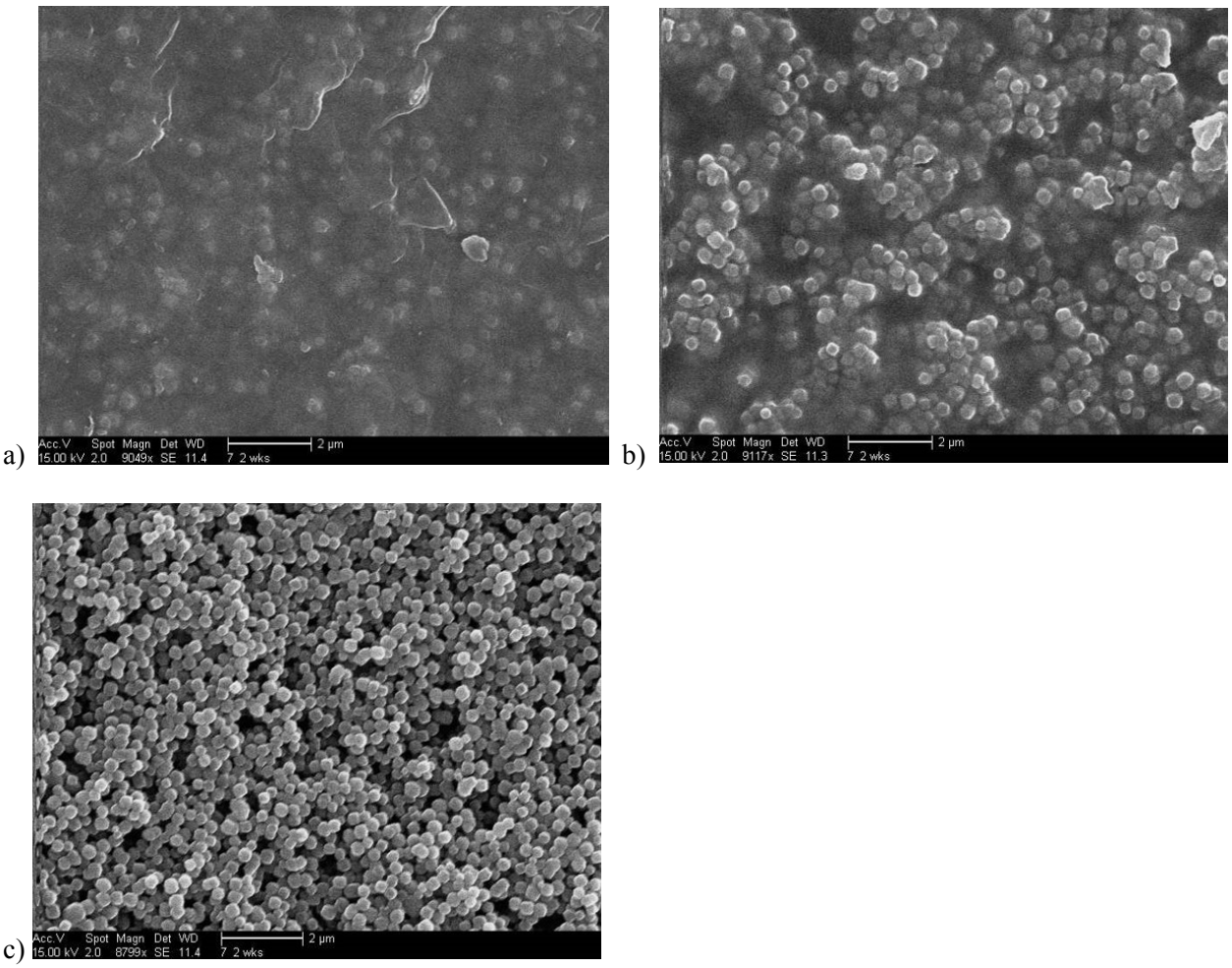

Figure S15. SEM top-down images of UiO-66/**SBS** MMMs show increasing UiO-66 content uniformly encased in polymer at a) 30 and b) 50 wt% loadings. At c) 90 wt% loadings, the MOF appears more isolated and film surfaces roughen accordingly. All scale bars are 2 µm.

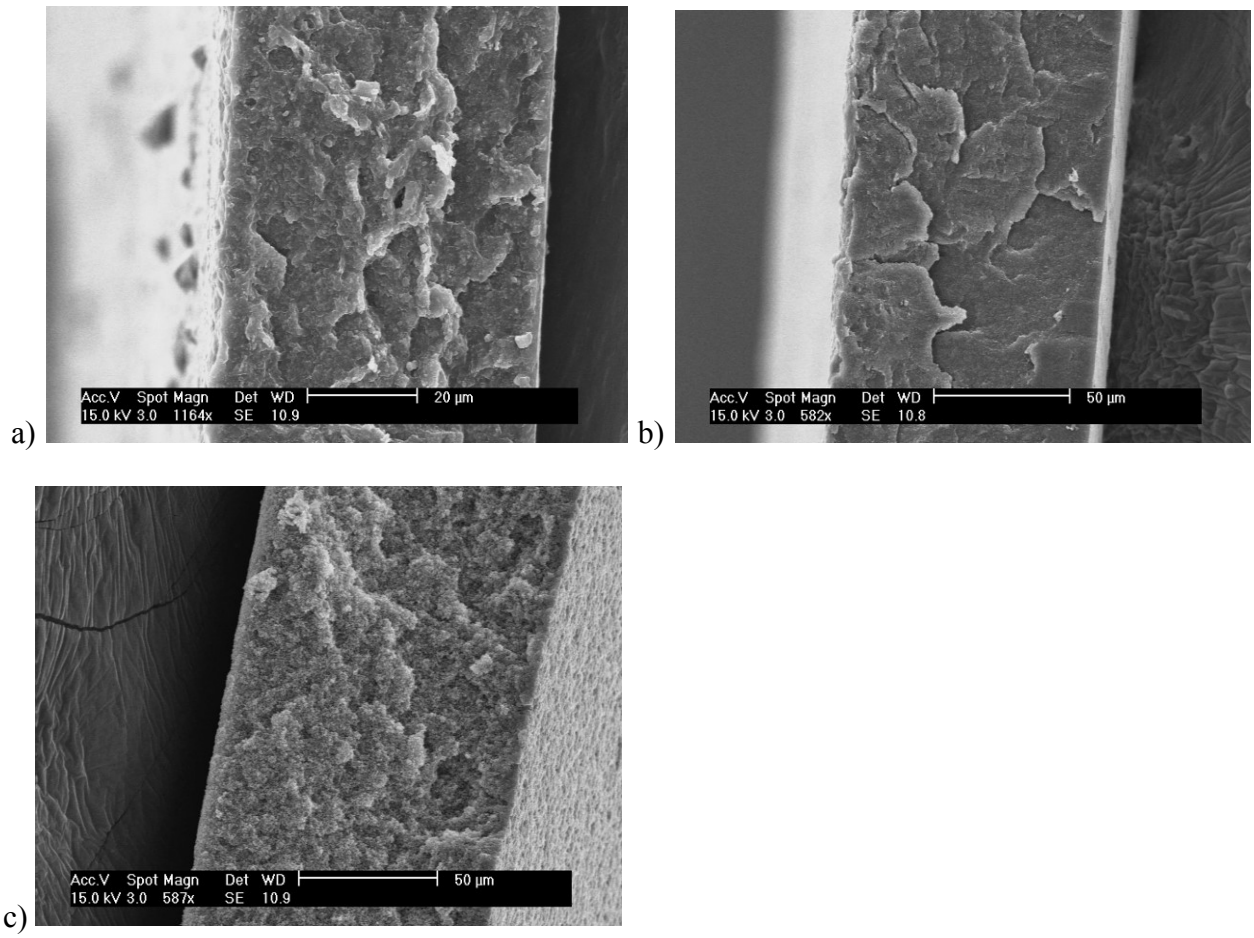

Figure S16. SEM cross-sectional images of UiO-66/**SBS** MMMs show increasing UiO-66 content uniformly dispersed in polymer at a) 30 (scale bar = 20 µm) b) 50 (scale bar = 50 µm) and c) 90 wt% (scale bar = 50 µm) loadings.

a) 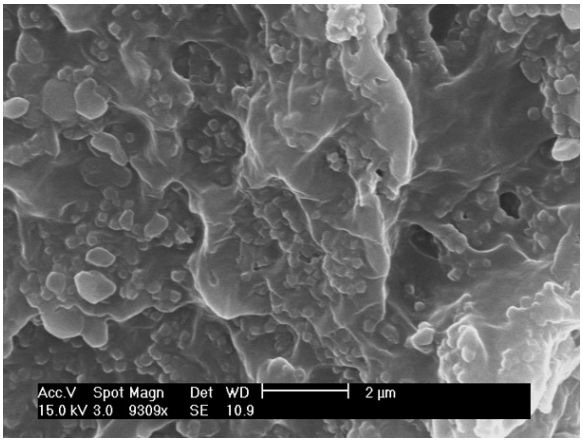

b) 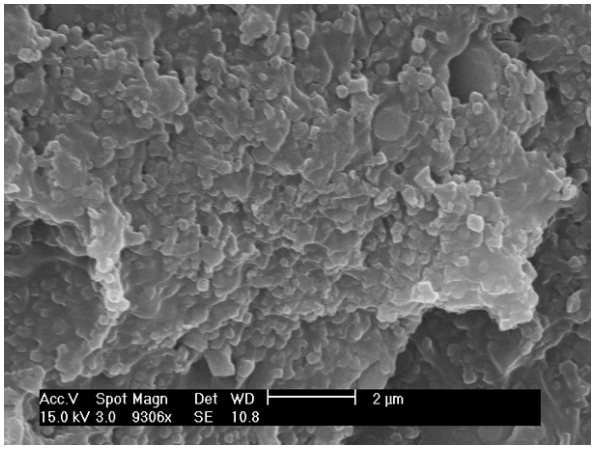

c) 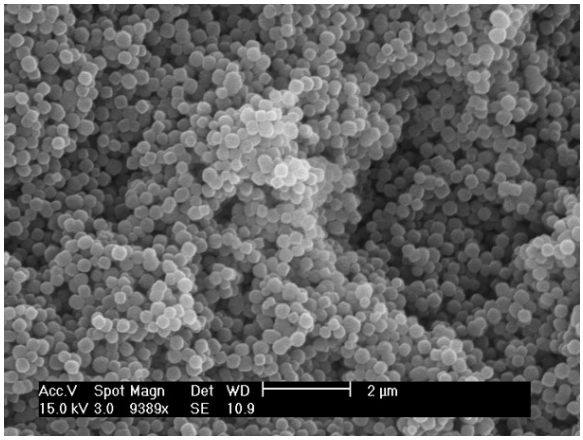

Figure S17. SEM cross-sectional zoomed-in images of UiO-66/**SBS** MMMs show increasing UiO-66 content uniformly encased in polymer at a) 30 and b) 50 wt% loadings. At c) 90 wt% loading, the MOF appears more isolated, showing a much more porous overall morphology throughout the cross-section. All scale bars are 2 µm.

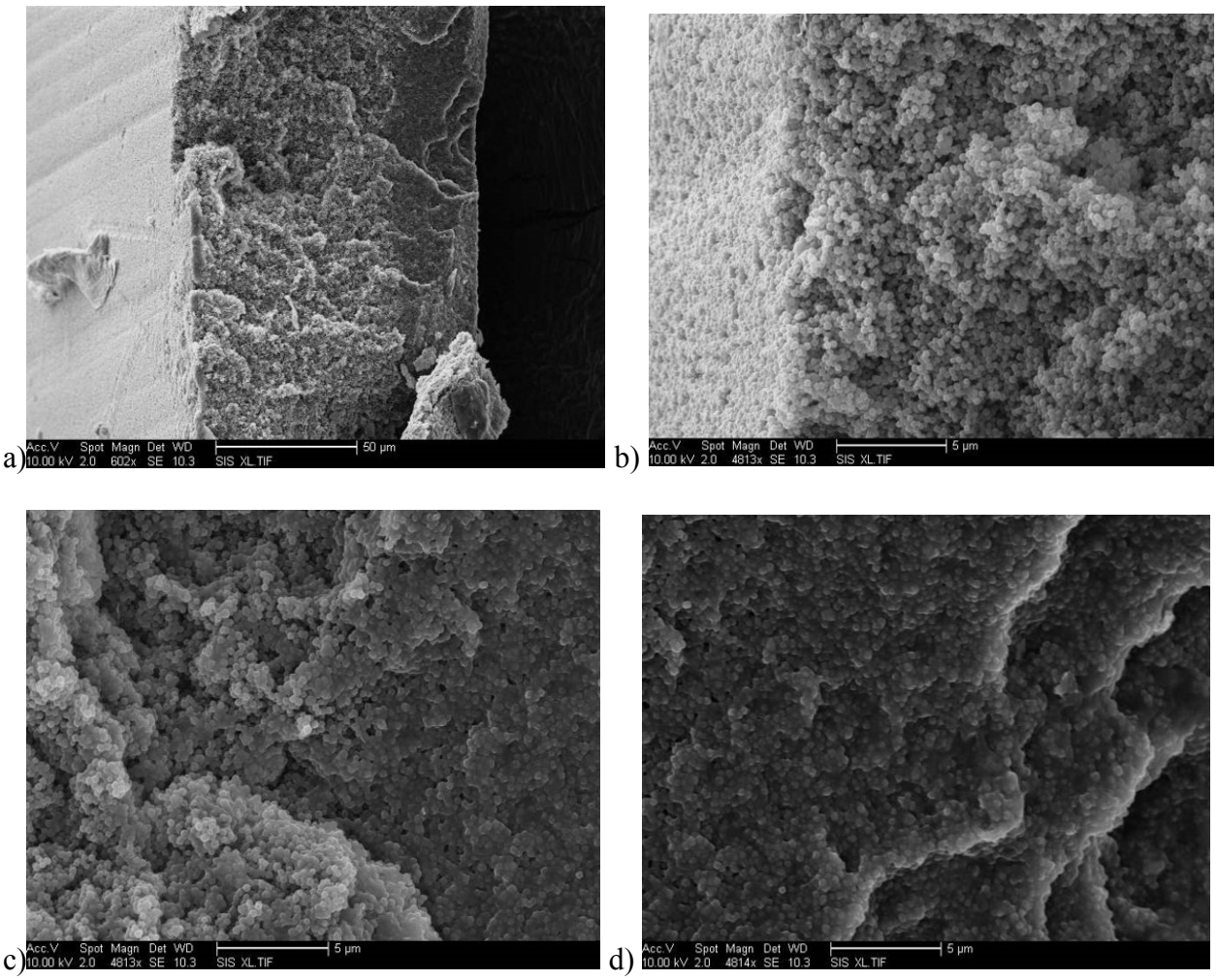

Figure S18. SEM cross-sectional images of a) 70 wt% UiO-66/**SBS** MMMs show two distinct membrane morphologies in a single membrane (scale bar = 50 µm). Zoomed-in image (b) shows the rougher morphology seen in higher MOF loadings **(**Figure S18c), c) shows both morphologies in a single image (rough on the left, dense on the right). Image d) shows the dense morphology similar to lower MOF loadings **(**Figures S18a, S18b**).** Scale bars of images b-d are all 5 µm.

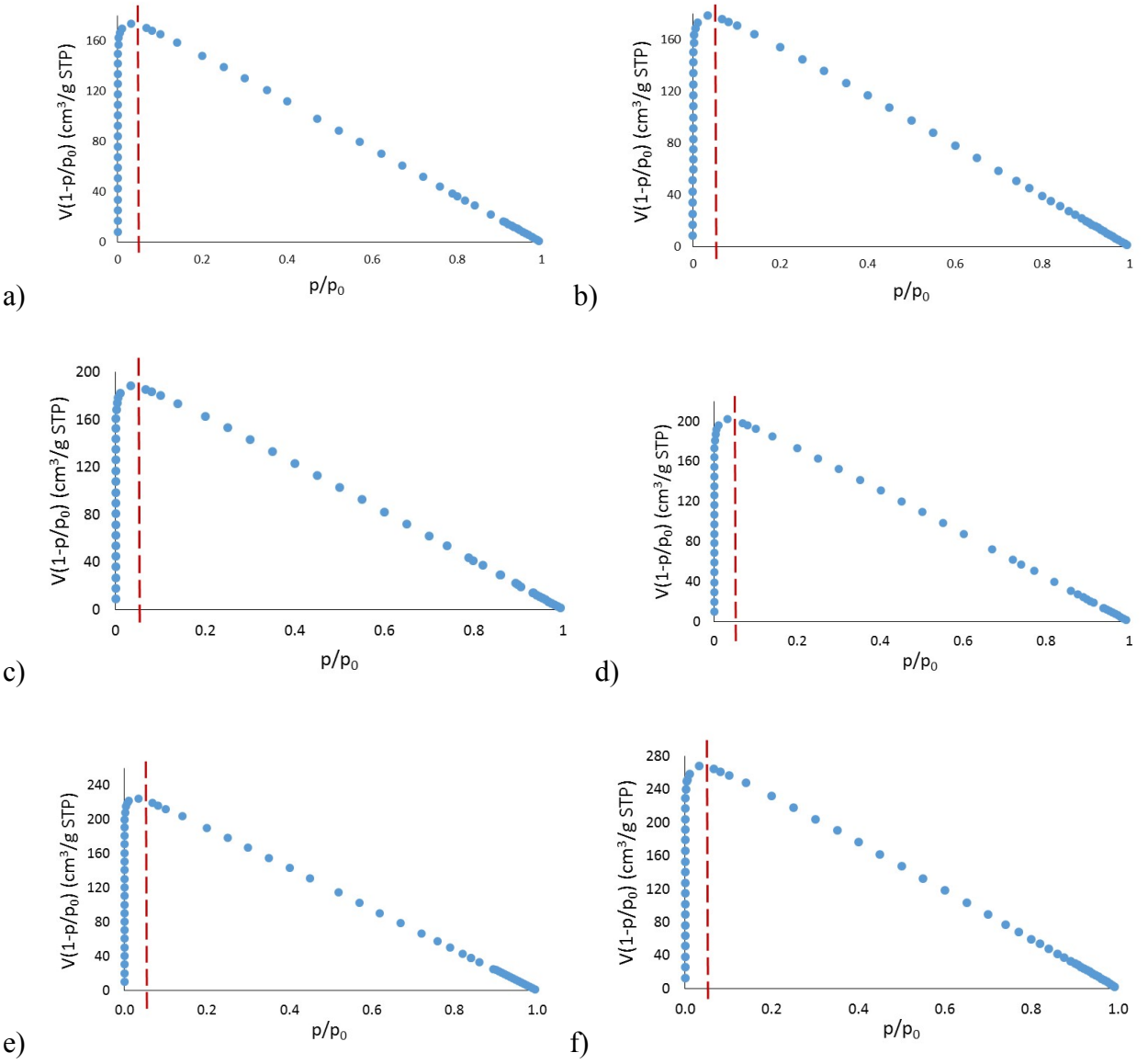

Figure S19. Representative Rouquerol plots from several MMMs. The dashed lines on the Rouquerol plots designate the upper limit of data used for calculating the BET surface areas of the respective materials, demonstrating compliance with criteria II. Ten data points were used for each BET surface area measurement. Rouquerol plots of: a) 70 wt% UiO-66/**SBS**, b) 80 wt% UiO-66/**SBS**, c) 90 wt% UiO-66/**SBS**, d) 70 wt% UiO-66/**PS**, e) 70 wt% UiO-66/**SBR** and f) solid UiO-66.

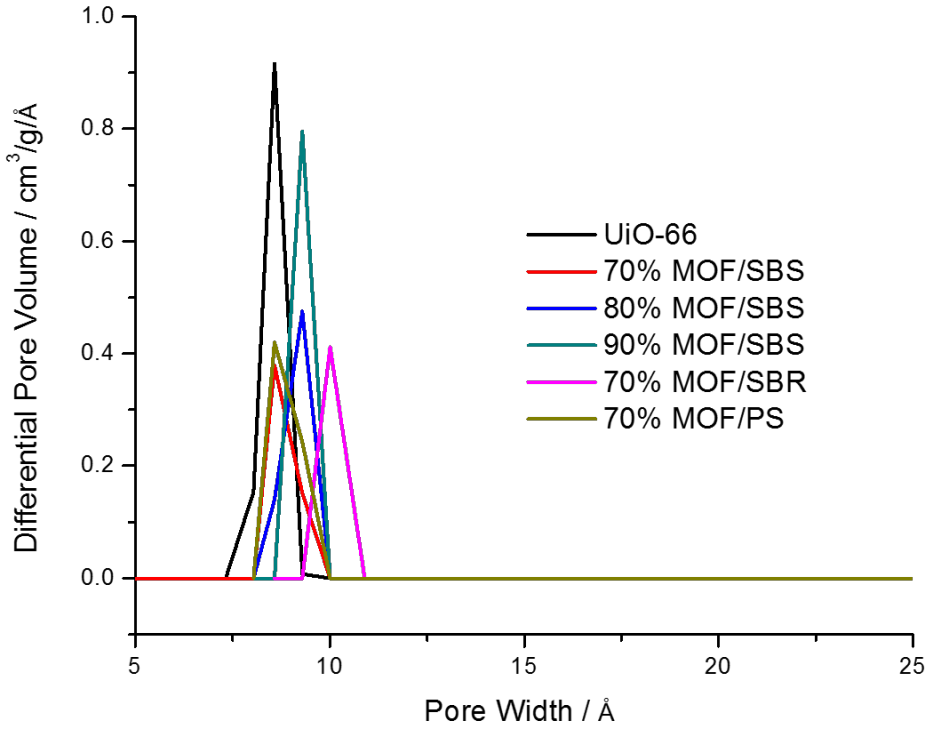

Figure S20. Pore size distributions of several MMMs. Preservation of the ~8.5 Å pore of the native MOF is seen in all MMMs. Differential pore size distribution is calculated by the DFT method.

a)  b) 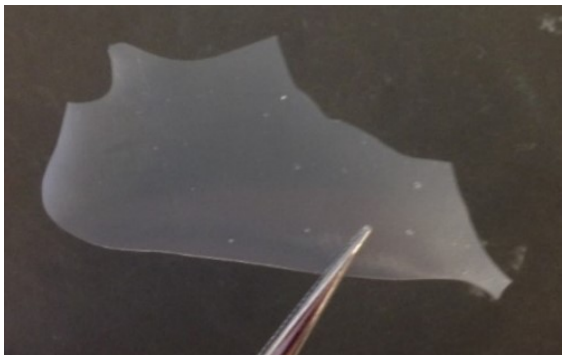

Figure S21. Photographs of a) a 50 wt% UiO-66/**PS** film and b) a fragment of the film, demonstrating its extreme brittleness, which prevented mechanical testing.

a)  b) 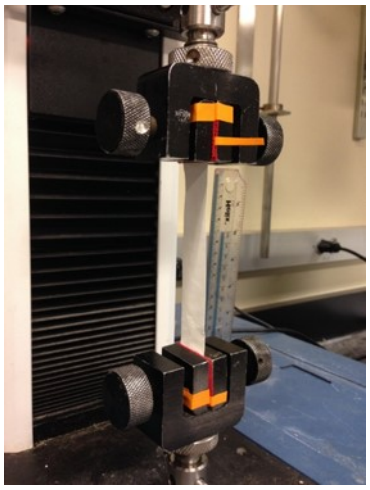

Figure S22. Membranes of a) 30 wt% UiO-66/**SBR** demonstrate the deformation of **SBR**-based films upon delamination. This deformation limits their utility and hinders mechanical testing. At b) 70 wt%, however, UiO-66/**SBR** membranes were sufficiently robust to withstand mechanical testing, seen here in the ASTM testing instrument.

a)  b) 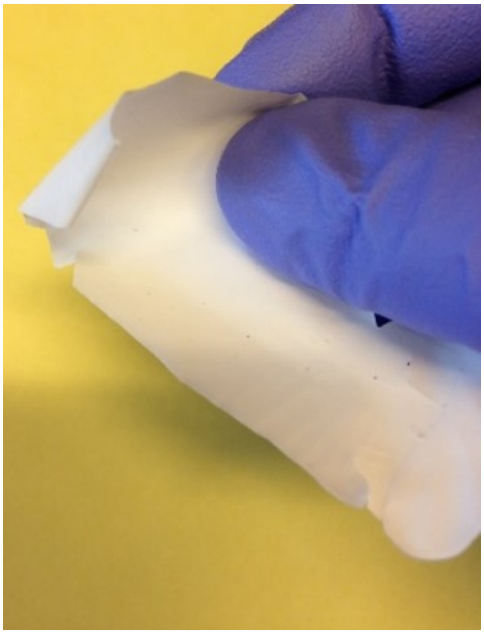

Figure S23. SBS-based MMMs: a) 70 wt% UiO-66, b) 80 wt% UiO-66 do not deform or crack upon delamination, and can withstand normal handling as well as mechanical testing.

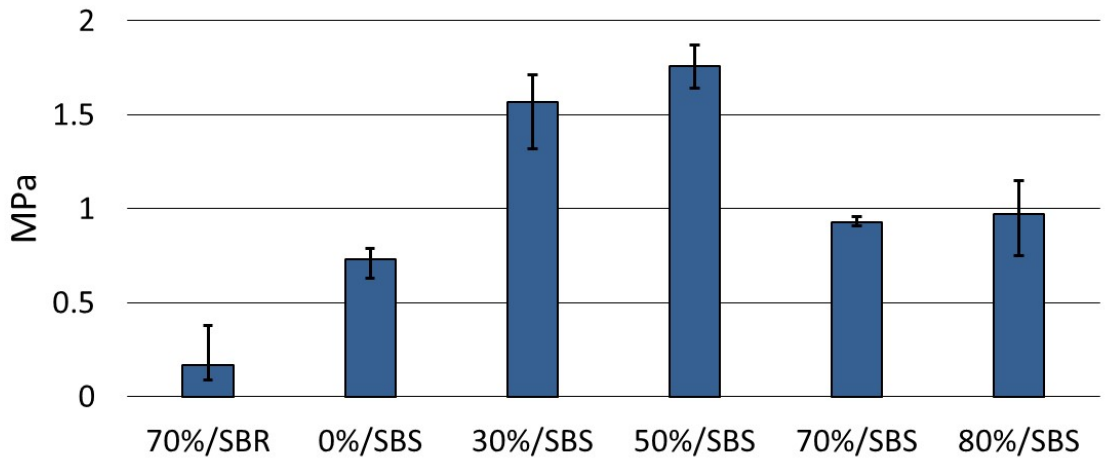

Figure S24. Ultimate tensile strength (UTS) of several MMMs. **SBS**-based MMMs at all loadings tested show better performance than the 70 wt% UiO-66/**SBR** MMM. All **SBS** MMMs tested show better ultimate tensile strength than the starting **SBS**. All measurements are the average of at least three independent membranes.

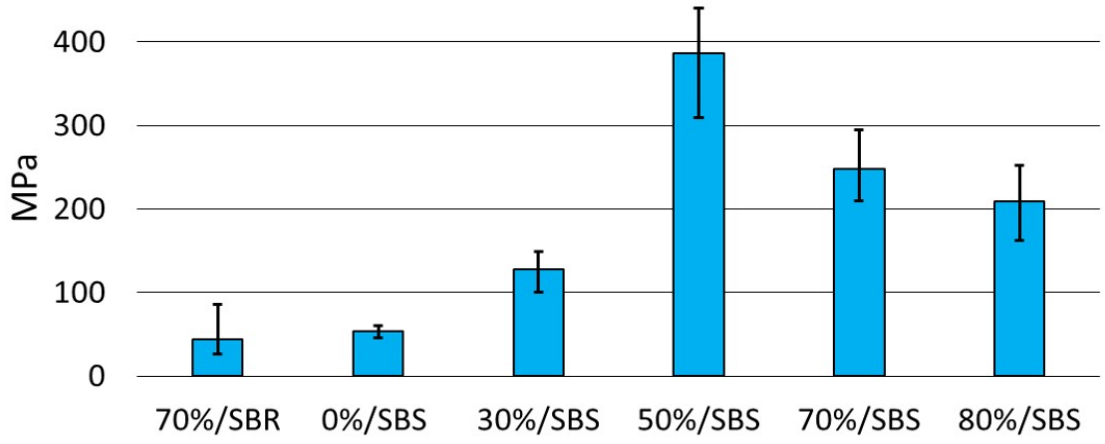

Figure S25. Elastic modulus of several MMMs. **SBS**-based MMMs at all loadings tested perform at least as well as the 70 wt% UiO-66/**SBR** MMM. All **SBS** MMMs tested show a higher elastic modulus than the starting polymer. All measurements are the average of at least three independent membranes.

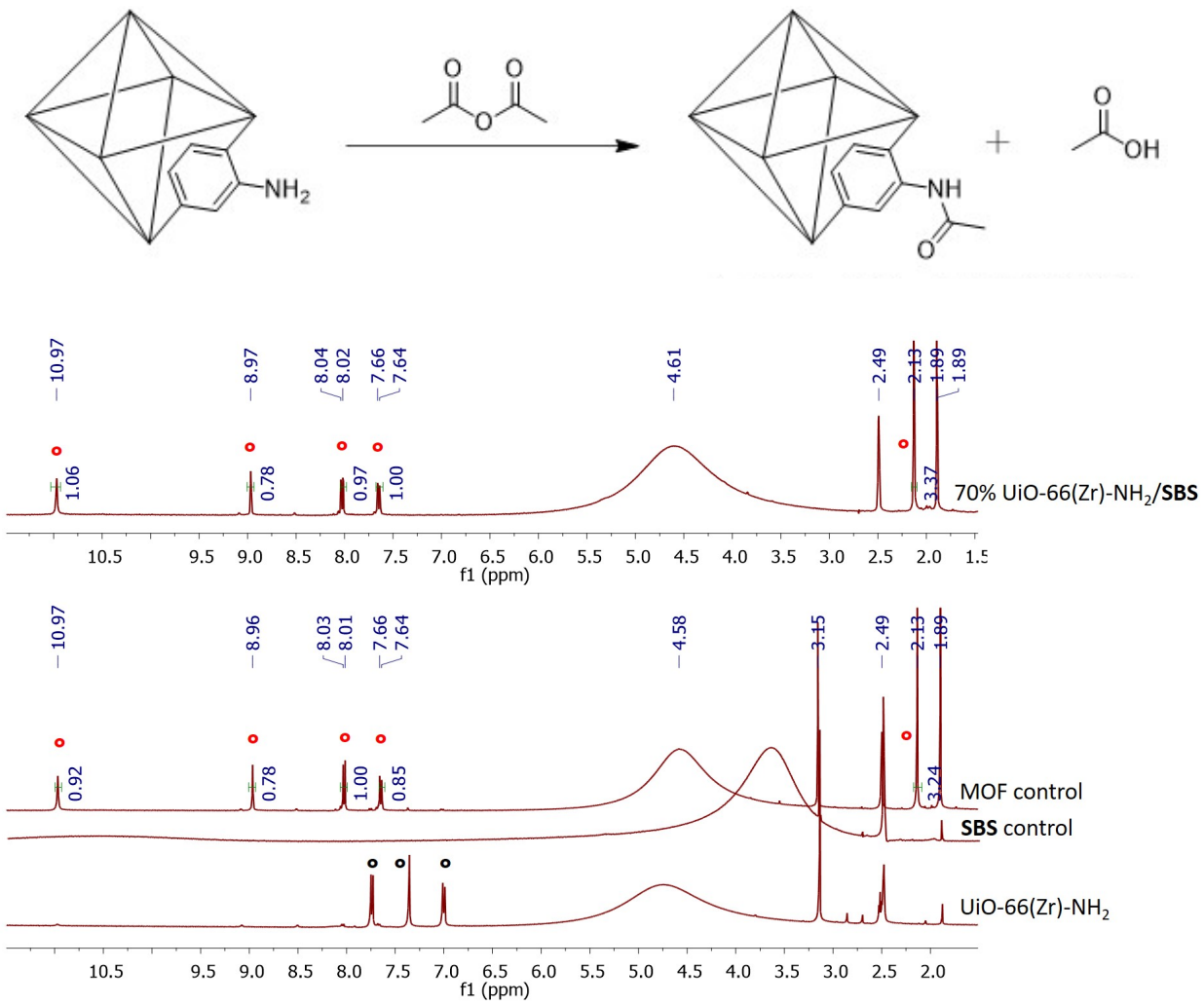

Figure S26. Ligand PSM experiments on MMMs. *Top*: Scheme illustrating the PSM reaction where UiO-66-NH_2 is immersed in acetic anhydride resulting in acetylation of the 2-aminoterephthalate ligand in the UiO-66-NH_2 lattice, forming UiO-66-AM1. NMR traces show the MOF starting material, MOF-only and polymer-only controls and the 80 wt% UiO-66/**SBS** MMM tested. Unmodified 2-aminoterephthalate phenyl peaks are indicated with black circles; acetylated 2-aminoterephthalate peaks are indicated with red circles.

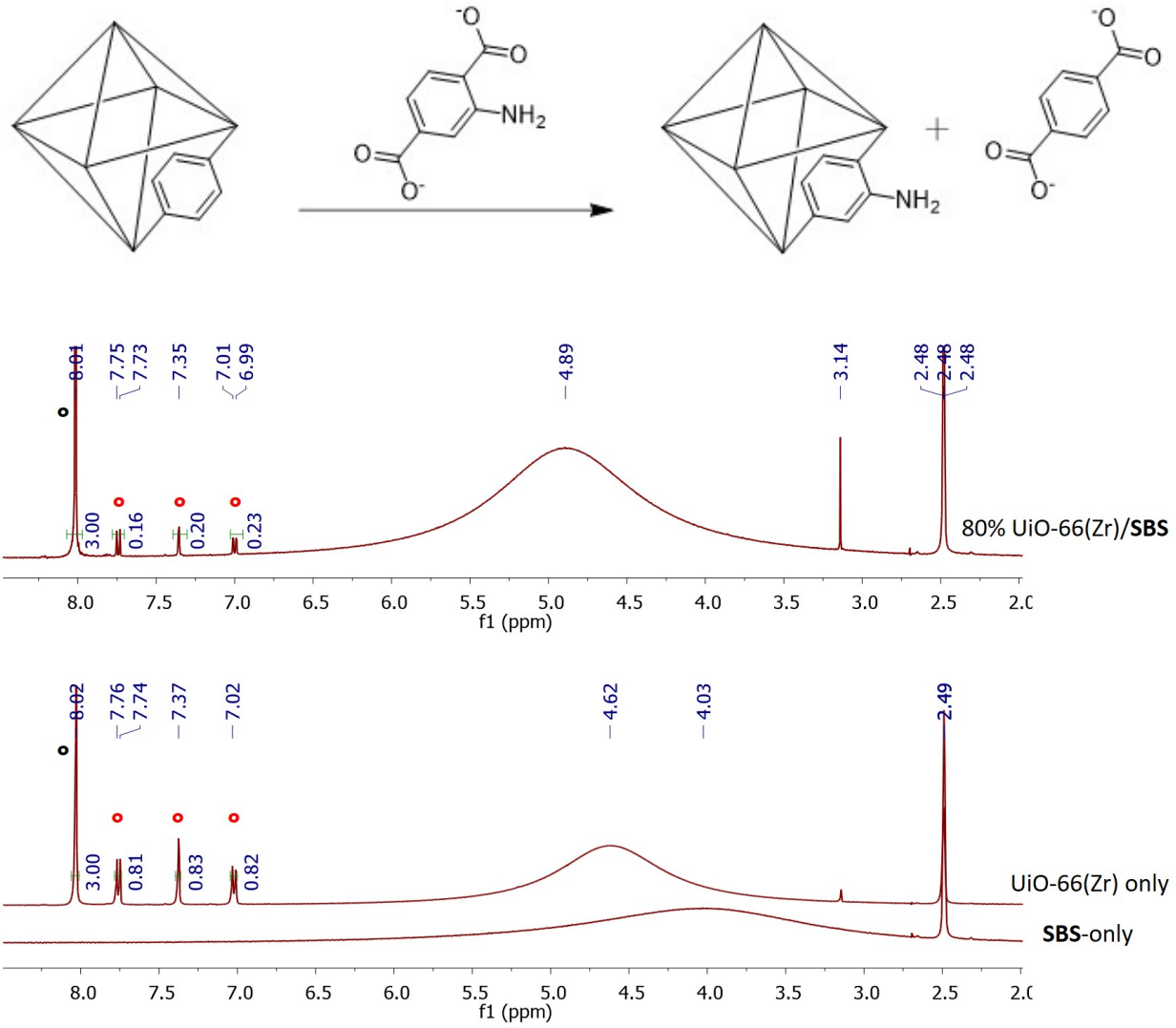

Figure S27. Ligand PSE experiments on MMMs. *Top*: Scheme illustrating the PSE reaction where UiO-66 is immersed in a solution of deprotonated 2-aminoterephthalate resulting in displacement of terephthalate from UiO-66 and incorporation of the 2-aminoterephthalate ligand into the UiO-66 lattice. NMR traces show MOF-only and polymer-only controls and the 80 wt% UiO-66/**SBS** MMM tested. Unmodified terephthalate phenyl peaks are indicated with black circles; 2-aminoterephthalate peaks are indicated with red circles.

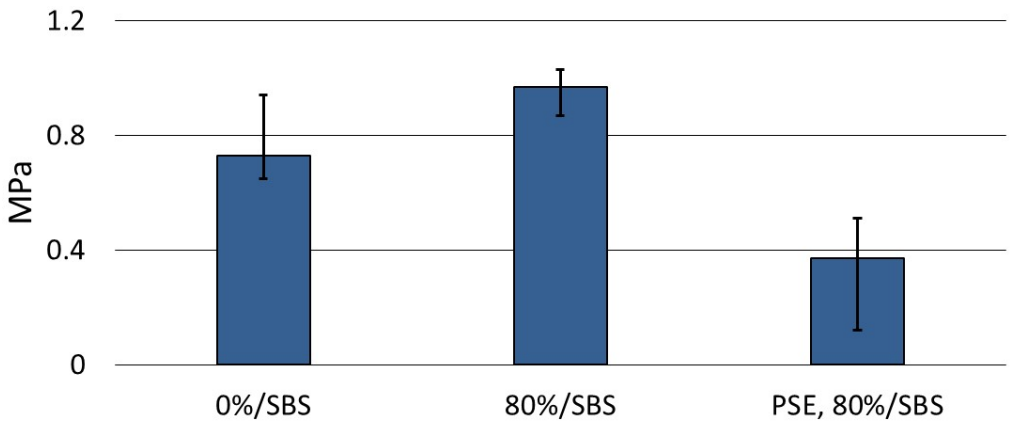

Figure S28. Ultimate tensile strength (UTS) of 80 wt% MOF/**SBS** MMM subject to PSE compared to untreated MMM and the starting polymer. Tensile strength diminishes notably post-PSE reaction. All measurements are the average of at least three independent membranes, except for the post-PSE MMM measurement (n=2).

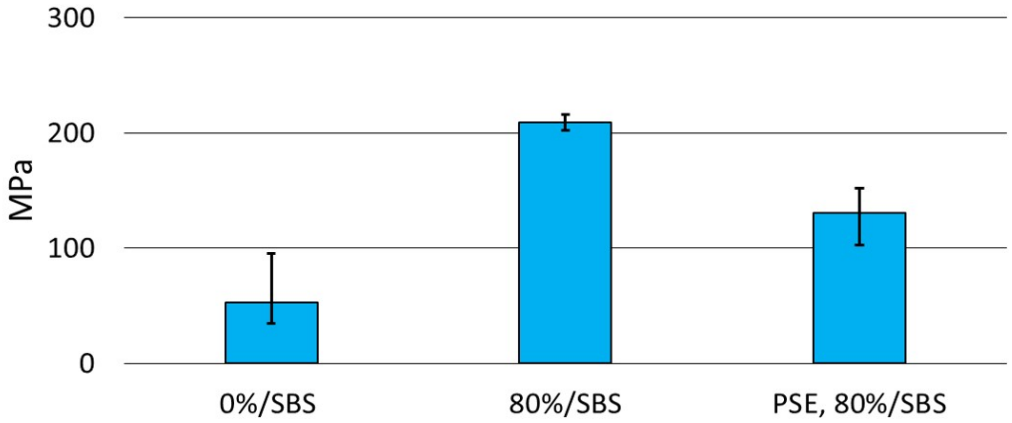

Figure S29. Elastic modulus of 80 wt% MOF/**SBS** MMM subject to PSE compared to untreated MMM and the starting polymer. Elastic modulus diminishes post-PSE reaction, yet remains higher than that of the starting polymer. All measurements are the average of at least three independent membranes, except for the post-PSE MMM measurement (n=2).

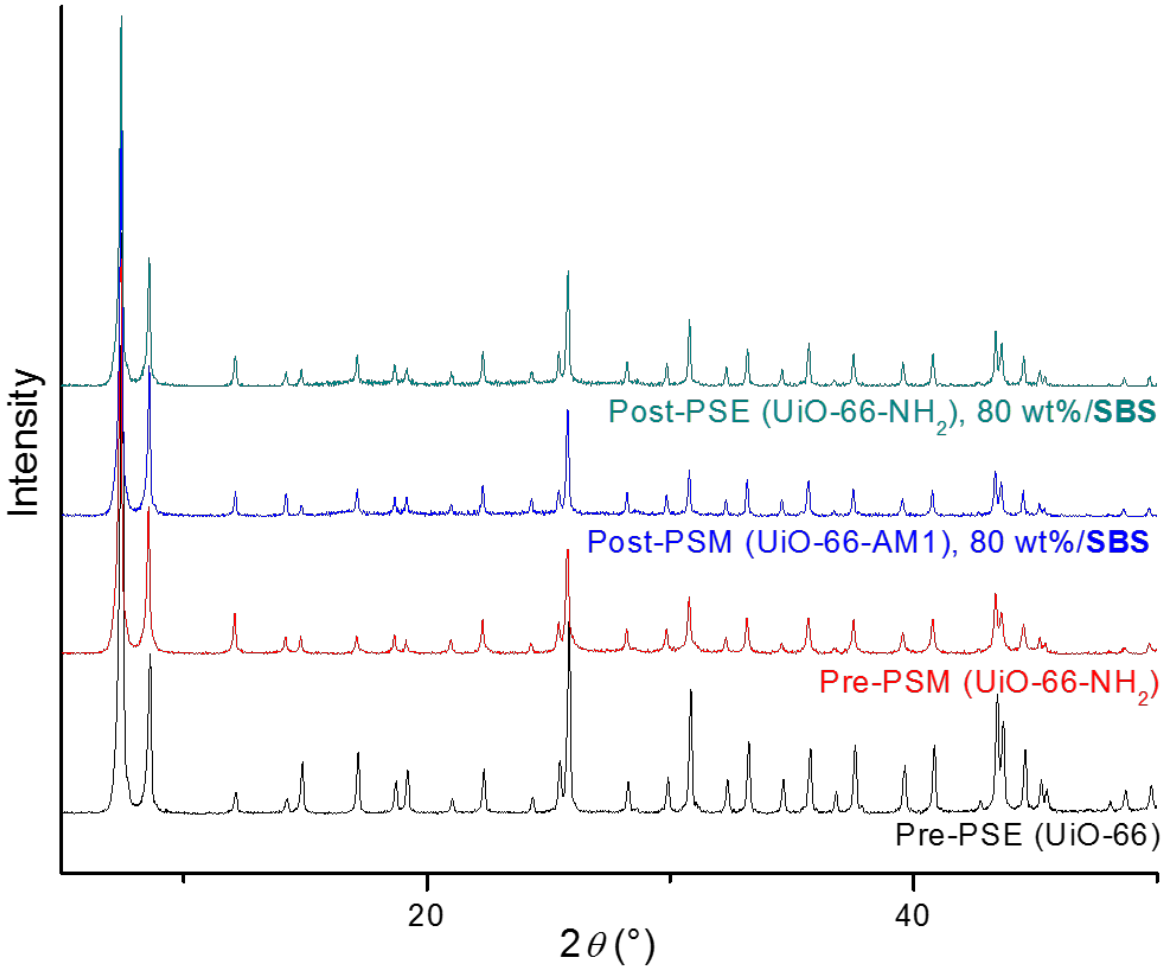

Figure S30. PXRD patterns of post-reaction 80 wt% UiO-66/**SBS** MMMs, compared to the starting MOFs. All powder patterns show that UiO-66 remains highly crystalline within the MMMs after reaction.

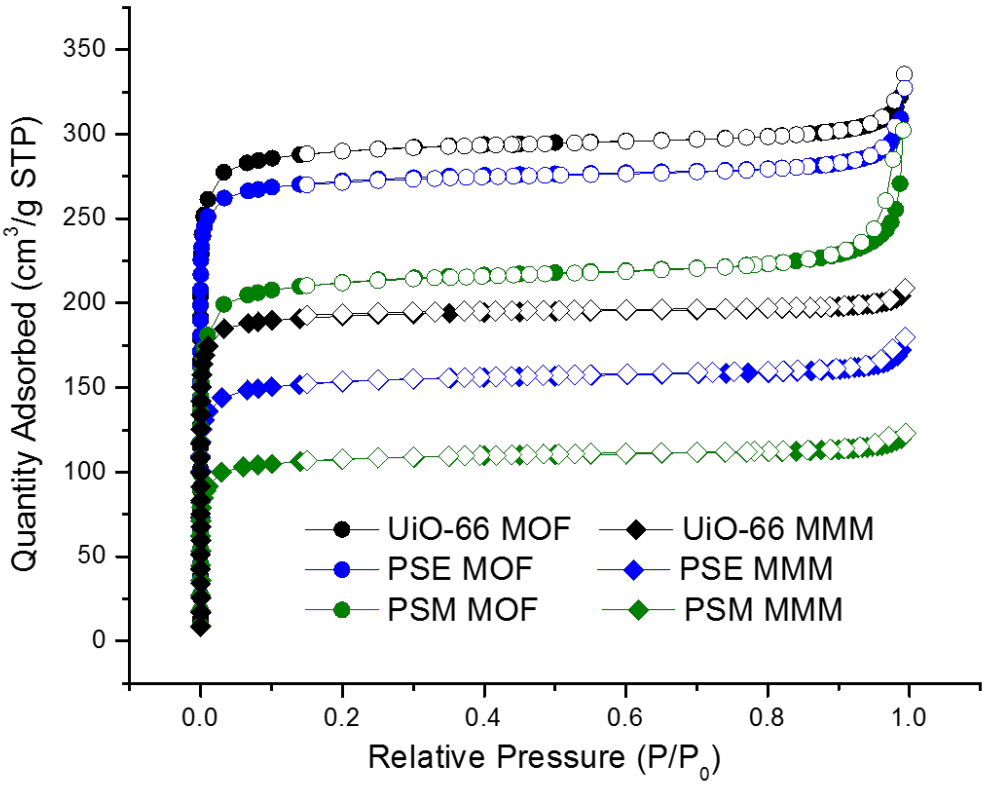

Figure S31. Nitrogen sorption isotherm data of post-reaction 80 wt% UiO-66/**SBS** MMMs, compared to post-reaction pure MOF controls. Black traces represent UiO-66 samples, blue traces represent post-PSE samples, and green traces represent post-PSM samples. Circle symbols represent MOF samples, while diamond symbols represent MMM samples. Closed symbols represent the adsorption branch, while open symbols represent the desorption branch of the respective isotherms.

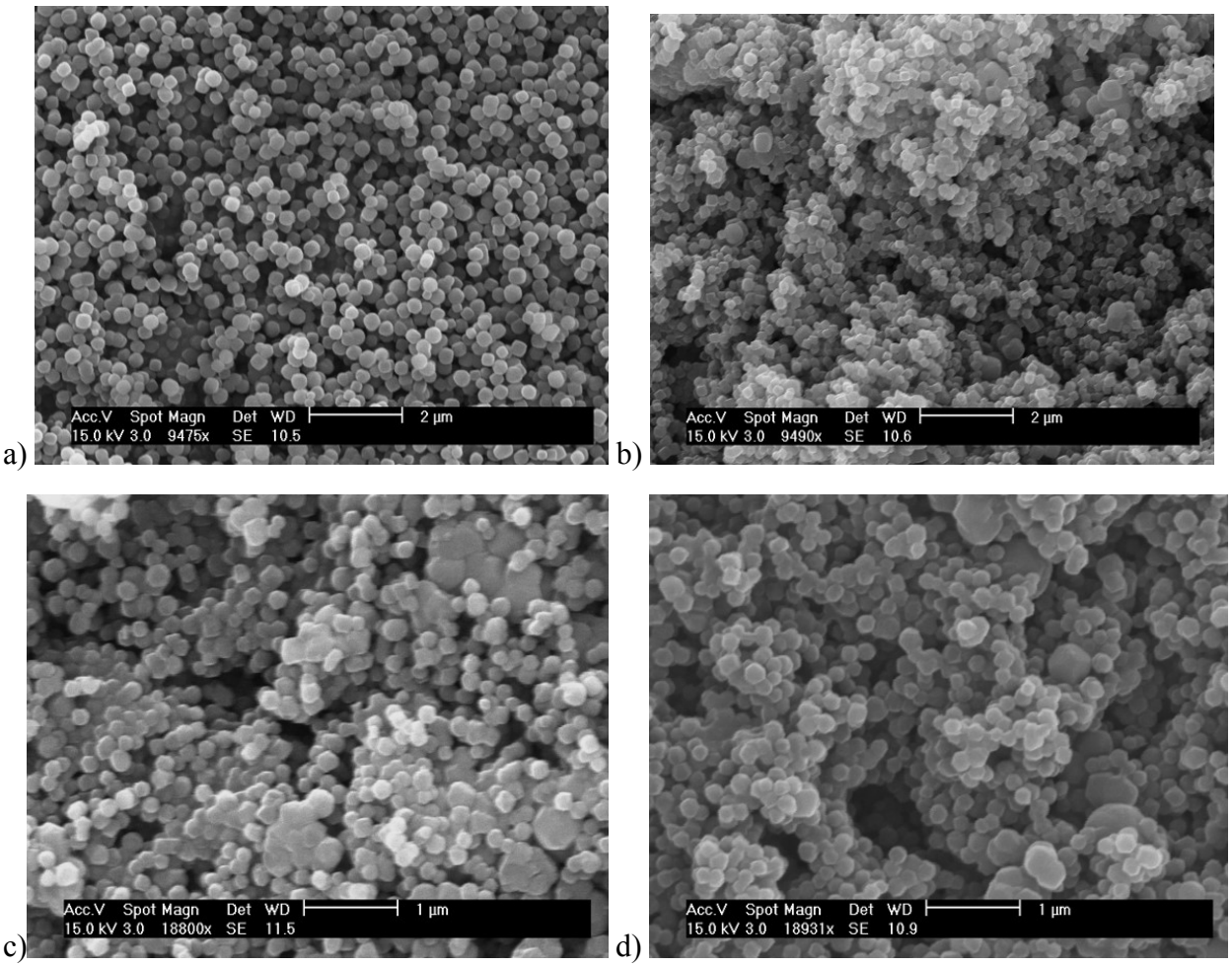

Figure S32. SEM images of MOF pre- and post- PSE and PSM reactions show no significant changes in morphology, as seen by comparing: a) native UiO-66 with b) post-PSE 80 wt% UiO-66/**SBS** MMM cross section, both with scale bars 2 µm, and c) native UiO-66-NH_2 with d) post-PSM 80 wt% UiO-66-NH_2/**SBS** MMM cross section, both with scale bars 1 µm.

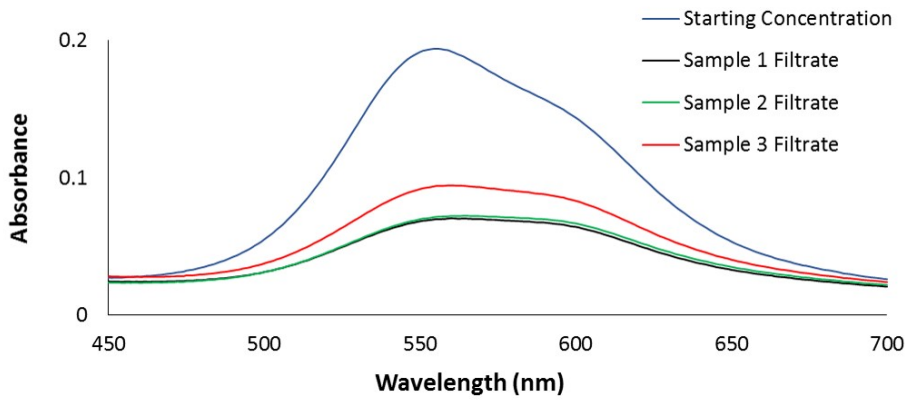

Figure S33. Coomassie Blue dye filtration using UiO-66/**SBS** MMMs. The three filtrations resulted in an average of 60±8% retention of the dye. Filtration experiments were conducted using three independent 80 wt% UiO-66/**SBS** membranes, delivering 2.5 mL of 10 μM Coomassie Brilliant Blue R-250 dye at a syringe rate of 0.1 mm/min.

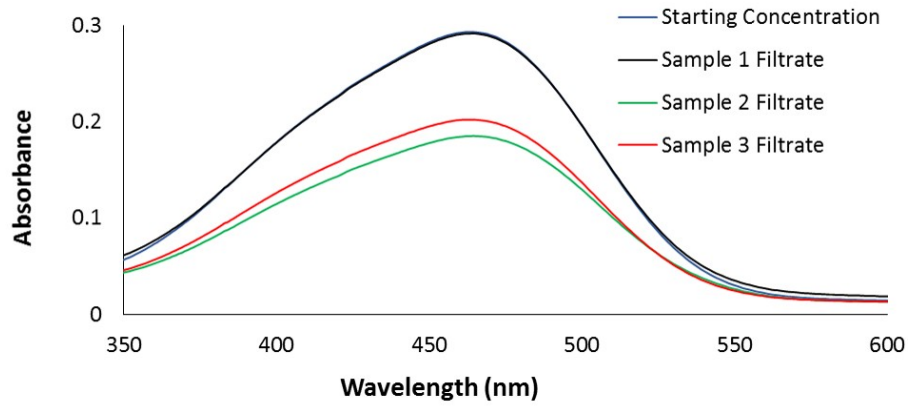

Figure S34. Methyl Orange dye filtration using UiO-66/**SBS** MMMs. The three filtrations resulted in an average of 23±22% retention of the dye. Filtration experiments were conducted using three independent 80 wt% UiO-66/**SBS** membranes, delivering 2.5 mL of 10 μM Methyl Orange dye at a syringe rate of 0.1 mm/min. Upon examination, the Sample 1 membrane showed fracture defects after filtration, likely resulting in its demonstrated 0% dye retention.

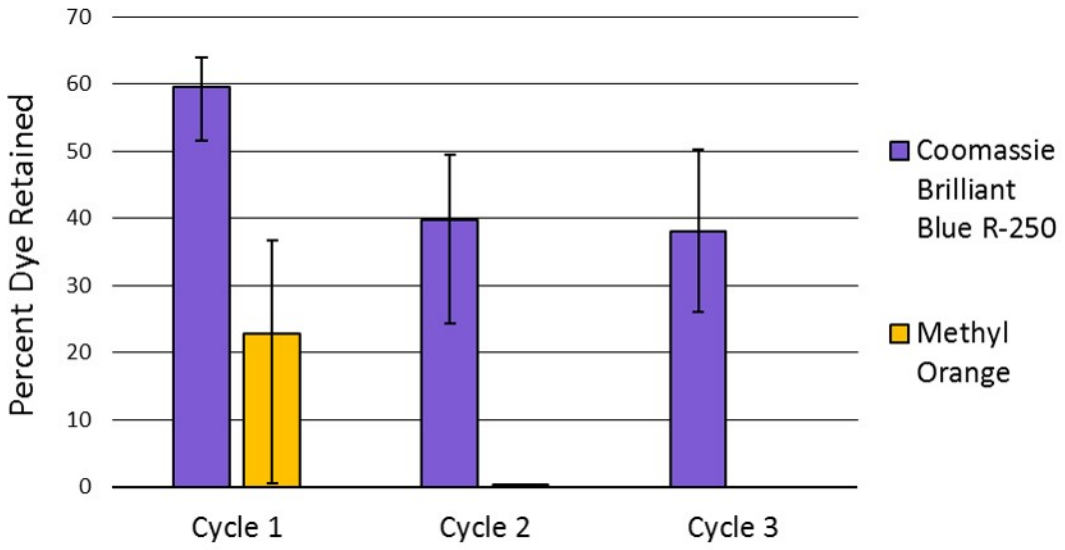

Figure S35. Recyclability tests of the three 80 wt% UiO-66/**SBS** MMMs tested for dye filtration. Cycle 1 data is the data shown in Figures S33 and S34, while Cycles 2 and 3 demonstrate the first and second reuse cycles, respectively. Upon examination of the Methyl Orange-tested MMMs after Cycle 2, all membranes showed fracturing consistent with 0% dye retention. Conversely, the Coomassie Blue-tested MMMs maintained their pristine form after three cycles, showing only slightly lowered dye retention abilities upon reuse.

References

1. J. Rouquerol, P. Llewellyn and F. Rouquerol, in *Studies in Surface Science and Catalysis*, eds. P. L. Llewellyn, F. Rodriquez-Reinoso, J. Rouqerol and N. Seaton, Elsevier, 2007, vol. 160, pp. 49-56.

2. D. A. Gómez-Gualdrón, P. Z. Moghadam, J. T. Hupp, O. K. Farha and R. Q. Snurr, *J. Am. Chem. Soc.,* 2016, **138**, 215-224.